

Experience-dependent dopamine modulation of male aggression

<https://doi.org/10.1038/s41586-024-08459-w>

Received: 20 January 2024

Accepted: 27 November 2024

Published online: 22 January 2025

 Check for updates

Bing Dai¹✉, Bingqin Zheng¹, Xiuzhi Dai¹, Xiaoyang Cui¹, Luping Yin¹, Jing Cai¹, Yizhou Zhuo^{2,3,4}, Nicolas X. Tritsch^{1,5,9}, Larry S. Zweifel^{6,7}, Yulong Li^{2,3,4} & Dayu Lin^{1,5,8}✉

Numerous studies support the role of dopamine in modulating aggression^{1,2}, but the exact neural mechanisms remain elusive. Here we show that dopaminergic cells in the ventral tegmental area (VTA) can bidirectionally modulate aggression in male mice in an experience-dependent manner. Although VTA dopaminergic cells strongly influence aggression in novice aggressors, they become ineffective in expert aggressors. Furthermore, eliminating dopamine synthesis in the VTA prevents the emergence of aggression in naive mice but leaves aggression intact in expert aggressors. VTA dopamine modulates aggression through the dorsal lateral septum (dLS), a region known for aggression control. Dopamine enables the flow of information from the hippocampus to the dLS by weakening local inhibition in novice aggressors. In expert aggressors, dLS local inhibition naturally weakens, and the ability of dopamine to modulate dLS cells diminishes. Overall, these results reveal a sophisticated role of dopamine in the rise of aggression in adult male mice.

Aggression is an innate social behaviour that is essential for defending territory, competing for resources and securing mates. Extensive research has revealed a subcortical core aggression circuit that is composed of the medial hypothalamus, extended amygdala and periaqueductal gray³. A parallel set of studies suggests that dopamine has a complex role in modulating aggression^{1,2}. First, dopamine receptor antagonists represent the most frequent and enduring treatment for suppressing aggression in humans⁴. Typical antipsychotics, which mainly target D2 receptors (D2Rs), have been used for decades to control aggression associated with psychotic conditions such as schizophrenia, autism and borderline personality disorders⁵. However, their effects are closely linked to sedation, raising the question of whether diminished aggression is secondary to the general suppression of arousal⁶. Furthermore, stimulants that increase central dopamine levels, such as amphetamine and methamphetamine, can heighten aggression, although a meta-analysis found that this effect was highly variable depending on dosage and behavioural paradigms⁷.

Pharmacological studies in animals support a similarly complex role for dopamine in modulating aggression. Whereas early studies generally concluded that stimulants enhance aggression in rodents^{8,9}, more recent studies suggest that their effects vary with drug dosage and behavioural history¹⁰. D2R antagonists strongly reduce aggression in mice, but often concomitantly affect locomotion^{11,12}. The most perplexing finding is that D2R agonists, just like D2R antagonists, suppress aggression and reduce locomotion¹³. Genetic studies provide more uniform support for the role of dopamine in aggression. Mutations in monoamine oxidase A and catechol-*O*-methyltransferase

that impair the degradation of monoamines (including dopamine, serotonin and noradrenaline) are consistently linked to hyperaggressive phenotypes in humans^{14,15}. Similarly, monoamine oxidase A, catechol-*O*-methyltransferase and dopamine transporter (DAT) knockout mice all show increased dopamine levels in the central nervous system and abnormally high levels of inter-male aggression^{14,16,17}.

Previous circuit studies suggest that VTA dopaminergic cells can influence male aggression^{18,19}. One study showed that basal forebrain GABAergic (GABA refers to γ -aminobutyric acid) inputs to the lateral habenula (LHb) bidirectionally control attack and the valence of aggressive interaction in male mice²⁰. Given the dense projections from the LHb to the VTA, the VTA was considered to be a likely downstream region to mediate LHb modulation of aggression²¹. Indeed, another study reported that 10-min optogenetic activation of VTA dopaminergic cells enhanced attack towards conspecific intruders in male mice¹⁹. It has been suggested that VTA dopaminergic cells influence aggression by inhibiting the lateral septum¹⁸. However, paradoxically, VTA dopaminergic cells project mainly to the dLS²², a site that has been proposed to promote aggression through its inhibitory projection to the ventral lateral septum (vLS), which, in turn, inhibits the ventrolateral part of the ventromedial hypothalamus (VMHvl), a key site for aggression generation^{23–25}. Thus, although dopamine has been linked to aggression in numerous clinical and preclinical studies, its exact action remains unclear.

Here we show that whether VTA dopamine modulates aggression depends strongly on fighting experience. We then uncover the neural circuit mechanisms that underlie this experience-dependent dopamine modulation.

¹Neuroscience Institute, New York University Grossman School of Medicine, New York, NY, USA. ²State Key Laboratory of Membrane Biology, Peking University School of Life Sciences, Beijing, China. ³PKU-IDG/McGovern Institute for Brain Research, Beijing, China. ⁴Peking–Tsinghua Center for Life Sciences, Beijing, China. ⁵Department of Neuroscience and Physiology, New York University Grossman School of Medicine, New York, NY, USA. ⁶Department of Psychiatry and Behavioral Sciences, University of Washington, Seattle, WA, USA. ⁷Department of Pharmacology, University of Washington, Seattle, WA, USA. ⁸Department of Psychiatry, New York University Grossman School of Medicine, New York, NY, USA. ⁹Present address: Department of Psychiatry, Douglas Hospital Research Centre, McGill University, Montreal, Quebec, Canada. ✉e-mail: bd1409@nyu.edu; Dayu.Lin@nyulangone.org

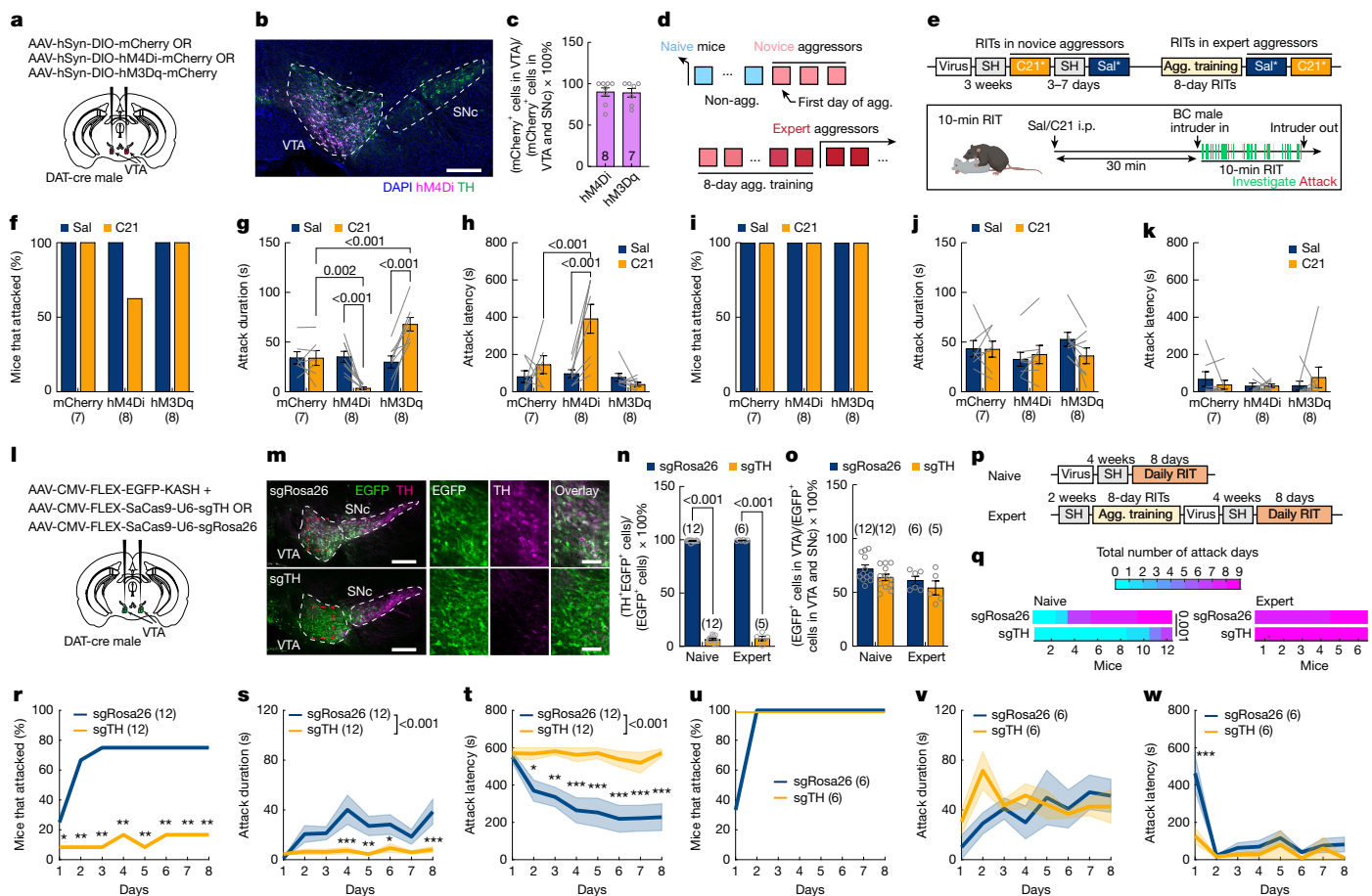


Fig. 1 | VTA^{DAT} cells modulate male aggression in naive mice and novice aggressors, but not in expert aggressors. **a**, Experimental design. **b**, Representative histology. Scale bar, 250 μ m. **c**, Percentage of total infected cells in the VTA. **d**, Definition of naive mice, novice aggressors and expert aggressors. **e**, Experimental timeline (top) and 10-min RI test (RIT; bottom). i.p., intraperitoneal; Sal, saline; SH, single housing; asterisk denotes counterbalanced. **f–k**, Percentage of mice that attacked (**f,i**), attack duration (**g,j**), and latency to attack (**h,k**) after saline or C21 treatment in mCherry, hM4Di and hM3Dq novice (**f–h**) and expert (**i–k**) aggressors. If no attack occurs, the latency is 600 s. **l**, Experimental design. **m**, Representative histology. Right images are enlarged views of the boxed areas. Scale bars, 250 μ m (left); 100 μ m (right). **n**, Percentage of TH-positive cells among EGFP-positive VTA cells in sgRosa26 and sgTH mice. **o**, Percentage of infected cells in the VTA in combined infected cells in the VTA and SNc. **p**, Experimental timeline. **q**, Number of attack days in 8-day RI tests in Rosa26 and sgTH naive mice (left) and in expert

aggressors (right). **r–w**, Percentage of attacking mice (**r,u**), attack duration (**s,v**) and latency to attack (**t,w**) during each daily RI test after ablating Rosa26 or TH in naive male mice (**r–t**) and in expert aggressors (**u–w**). * $P < 0.05$, ** $P < 0.01$, *** $P < 0.001$. Numbers in parentheses indicate numbers of mice. Circles and lines represent data from individual mice. **c,q**, Mann–Whitney test; **f**, McNemar’s test for hM4Di group; **g,h,j,k**, repeated-measures two-way ANOVA with multiple comparisons and Bonferroni’s or Tukey’s correction; **n,o**, two-way ANOVA with multiple comparisons and Bonferroni’s correction; **r,u**, Fisher’s exact tests with false discovery rate (FDR) correction; **s,t,v,w**, repeated-measures two-way ANOVA with multiple comparisons and Bonferroni’s correction. See Supplementary Table 1 for statistical details. Elements (mice) in **e** were created using BioRender (<https://biorender.com>). In this and all other figures, bars and error bars, and solid lines and shades, represent mean \pm s.e.m.; all $P \leq 0.05$ are indicated, if not, $P > 0.05$; all statistical tests are two-tailed. Brain illustrations are adapted from the Allen Brain Reference Atlas (<https://atlas.brain-map.org>).

VTA^{DAT} alters aggression only in novices

Optogenetic activation of VTA dopamine cells enhances attack and mounting in male mice¹⁹. However, the roles of these cells in naturally occurring inter-male aggression remain unclear. We thus chemogenetically inhibited VTA dopaminergic cells using hM4Di²⁶ (control: mCherry) in male DAT-Cre mice (Fig. 1a,b). More than 90% of infected cells were in the VTA (Fig. 1c). Pilot experiments suggested inconsistent changes in aggression after inhibiting DAT-expressing VTA (VTA^{DAT}) cells (data not shown). However, careful examination revealed that the mouse’s fighting experience might influence the manipulation outcome, which agrees with a previous report suggesting that D2R antagonists only suppress aggression in novice fighters²⁷. To investigate the role of experience-dependent dopamine modulation on aggression, we tested the effect of VTA^{DAT} inhibition in ‘novice’ and ‘expert’ aggressors (Fig. 1d,e). The former are defined as mice with fewer than

three days of attack experience, and the latter are mice with a minimum of eight days of continuous winning in the standard resident-intruder (RI) tests (Fig. 1d).

For novice aggressors, attack duration significantly decreased, and attack latency increased in hM4Di mice after injection of C21 (a hM4Di ligand)²⁸ compared with saline injection (Fig. 1f–h). Male and female investigation duration, mounting and intromission, latency to mount towards a female mouse and general locomotion in an open arena did not differ between C21- and saline-injected days (Extended Data Fig. 1c–e, i–l). mCherry control mice showed no change in any behaviours after C21 injection (Fig. 1f–h and Extended Data Fig. 1c–e, i–l). Thus, VTA^{DAT} inhibition suppresses aggression but not other behaviours in novice aggressors.

After the first round of C21 and saline injections, all mice underwent daily RI tests against BALB/c (BC) male intruders for another eight days to become expert aggressors, and were tested again (Fig. 1e). Unlike

the robust C21-induced decrease in aggression in novice aggressors, inhibiting VTA^{DAT} cells in expert aggressors did not impair aggressive behaviours. All mice attacked the BC intruders, and the attack duration and latency were comparable between C21- and saline-injected days (Fig. 1i–k). Investigation duration and locomotion also did not differ between C21- and saline-injected days (Extended Data Fig. 1f–h). Thus, VTA^{DAT} cells are crucial for aggressive behaviours in novices but not in expert aggressors.

We next asked whether chemogenetic activation of VTA^{DAT} cells can promote aggression, as optogenetic activation does^{18,19}, and if so, whether it depends on experience. We expressed hM3Dq in the VTA dopamine cells of DAT-Cre male mice and tested the aggression of novices and experts after saline and C21 injections (Fig. 1a,e). Chemogenetic activation of VTA^{DAT} cells consistently increased attack duration in novice aggressors without affecting attack latency and investigation duration (Fig. 1f–h and Extended Data Fig. 1c,d). Male sexual behaviours were unchanged after C21 injection (Extended Data Fig. 1i–l). By contrast, in expert aggressors, C21 injection did not alter attack duration or latency, further supporting an experience-dependent role for VTA^{DAT} cells in aggression (Fig. 1i–k). Notably, activation of VTA^{DAT} cells enhanced locomotion in both novice and expert aggressors, suggesting that C21 remains effective in changing VTA^{DAT} cell activity in expert aggressors and that the overall levels of aggression are dissociable from movement (Extended Data Fig. 1e,h).

The lack of change in aggression after manipulation of VTA^{DAT} in expert aggressors could not be explained by the ceiling or floor effects of aggression, because novice and expert aggressors attacked for a comparable amount of time, and the same manipulation readily altered attack duration in novice aggressors (Fig. 1g,j). The similar attack duration of novice and expert aggressors towards BC intruders is unsurprising. We recently found that although the level of aggression increases as mice gain more winning experience (reflected by their increased readiness to attack a stronger opponent), the attack duration towards a weak opponent—for example, a non-aggressive BC male intruder—plateaus after one to two days of winning²⁹. Nevertheless, to address whether aggressive behaviours were immune to perturbations in expert aggressors, we chemogenetically activated the *Esr1*-expressing population in the ventrolateral part of the ventromedial hypothalamus (VMHv^{Esr1}), a key population for driving aggression^{30,31} (Extended Data Fig. 2a–c). In contrast to the activation of VTA^{DAT} cells, activating VMHv^{Esr1} cells increased attack duration and shortened attack latency in both novice and expert aggressors (Extended Data Fig. 2d–f). Investigation duration also trended downwards after C21 injection, probably owing to increased aggression (Extended Data Fig. 2g). VMHv^{Esr1} activation also induced attacks towards female intruders, as previously reported^{30,32}, in both novice and expert aggressors (Extended Data Fig. 2h–k). By contrast, we never observed female-directed attacks after VTA^{DAT} activation (Extended Data Fig. 1m). Overall, our findings highlight the unique experience-dependent and target-specific modulatory effect of VTA^{DAT} cells on aggression.

Aggression is sexually dimorphic in mice³³. Virgin females generally show minimum aggression towards intruders. However, female aggression markedly increases during lactation, to protect the young—a phenomenon known as maternal aggression³³. We chemogenetically inhibited VTA^{DAT} cells in lactating females and found no significant change in any behavioural measures, including the probability of attack, attack duration and latency, investigation duration and locomotion (Extended Data Fig. 3a–h). Furthermore, chemogenetic activation of VTA^{DAT} cells did not change attack or social investigation in either virgin or lactating females (Extended Data Fig. 3i–m). However, VTA^{DAT} cell activation increased locomotion in females, as it did in males, suggesting that the manipulation was effective (Extended Data Fig. 3n). Thus, VTA^{DAT} cells are not essential for modulating female aggression, regardless of the reproductive state. We therefore focused our subsequent experiments on inter-male aggression.

Emergence of aggression requires VTA dopamine

We next asked whether dopamine is the key neurotransmitter in modulating aggression and, if so, whether its role is experience dependent. We induced mutagenesis of tyrosine hydroxylase (TH), a rate-limiting enzyme for dopamine synthesis, by injecting Cre-dependent CRISPR–SaCas9 and TH-targeting guide RNA (sgTH) (control: sgRosa26) virus into the VTA of DAT-Cre male mice that were either naive or had extensive winning experience³⁴ (Fig. 1l–p). Post hoc TH immunostaining confirmed the successful deletion of TH in sgTH-injected mice (Fig. 1m,n). Most virus-expressing cells were in the VTA, but some were also found in the substantia nigra pars compacta (SNc) (Fig. 1o).

Of the twelve naive sgTH males, none could attack consistently across eight days of the RI test; four attacked and achieved victories on some days but failed to maintain aggression in later days, whereas eight never attacked (Fig. 1q–t). By contrast, nine out of twelve control sgRosa26 mice showed escalated aggression over the first three RI tests and consistently attacked on subsequent testing days (Fig. 1q–t). The investigation duration of sgTH mice did not change over days, whereas it decreased gradually in sgRosa26 mice as aggression levels increased (Extended Data Fig. 4c). In expert aggressors, TH mutagenesis did not negatively affect aggression: both sgTH and sgRosa26 mice attacked the intruder reliably across days (Fig. 1q,u–w and Extended Data Fig. 4d). With regard to sexual behaviours, we found no difference between sgTH and sgRosa26 mice, regardless of their fighting experience. All males spent a similar time investigating and mounting females (Extended Data Fig. 4e–h).

In the open-field test, the maximum velocities of sgTH and sgRosa26 mice were comparable, but sgTH mice travelled less (Extended Data Fig. 4i–k), possibly owing to the virus spreading to the SNc, which is essential for spontaneous movement initiation³⁵ (Fig. 1m,o). Notably, the decrease in locomotion was similar for naive and expert aggressors, suggesting that the lack of stable aggression in sgTH naive mice is not tied to locomotor defects (Extended Data Fig. 4j). Thus, VTA dopamine is crucial for the emergence of aggression in naive mice. However, it is dispensable once aggression stabilizes after repeated fighting.

Aggression increase requires dopamine input to dLS

VTA dopamine must influence aggression by modulating downstream regions. On the basis of VTA^{DAT} cell projections²² and the relevance of candidate downstream regions to aggression^{18,23,24,36,37}, we focused on two structures: the dLS and the nucleus accumbens medial shell (NAcs). We first injected 6-hydroxydopamine (6-OHDA) (control: vehicle) bilaterally into the dLS or the NAcs to eliminate dopaminergic terminals in naive male mice (Fig. 2a). Histology confirmed that 6-OHDA led to a substantial decrease of dopaminergic terminals (Fig. 2b,c). Naive mice in which 6-OHDA was injected into the dLS did not develop stable aggression over repeated RI tests, in contrast with the escalated aggression over days that was seen in control and NAcs-lesioned mice (Fig. 2d and Extended Data Fig. 5a–d). In expert aggressors that underwent RI tests for eight days before the injection of 6-OHDA or vehicle into the dLS (Fig. 2e, top), minimal differences in aggression were observed between groups (Fig. 2e and Extended Data Fig. 5e–h). All expert aggressors continued to attack reliably over eight testing days (Fig. 2e). Thus, DA inputs to the dLS, but not to the NAcs, are essential for the emergence but not the maintenance of stable aggression.

dLS dopamine release over repeated fighting

We next recorded dLS dopamine fluctuations using the third-generation dopamine sensor, GRAB_{DA3h} (ref. 38) (Fig. 2f–n). Fibre photometry recording revealed a consistent increase in GRAB_{DA3h} in the dLS and the nucleus accumbens core (NAcc) after optogenetic activation

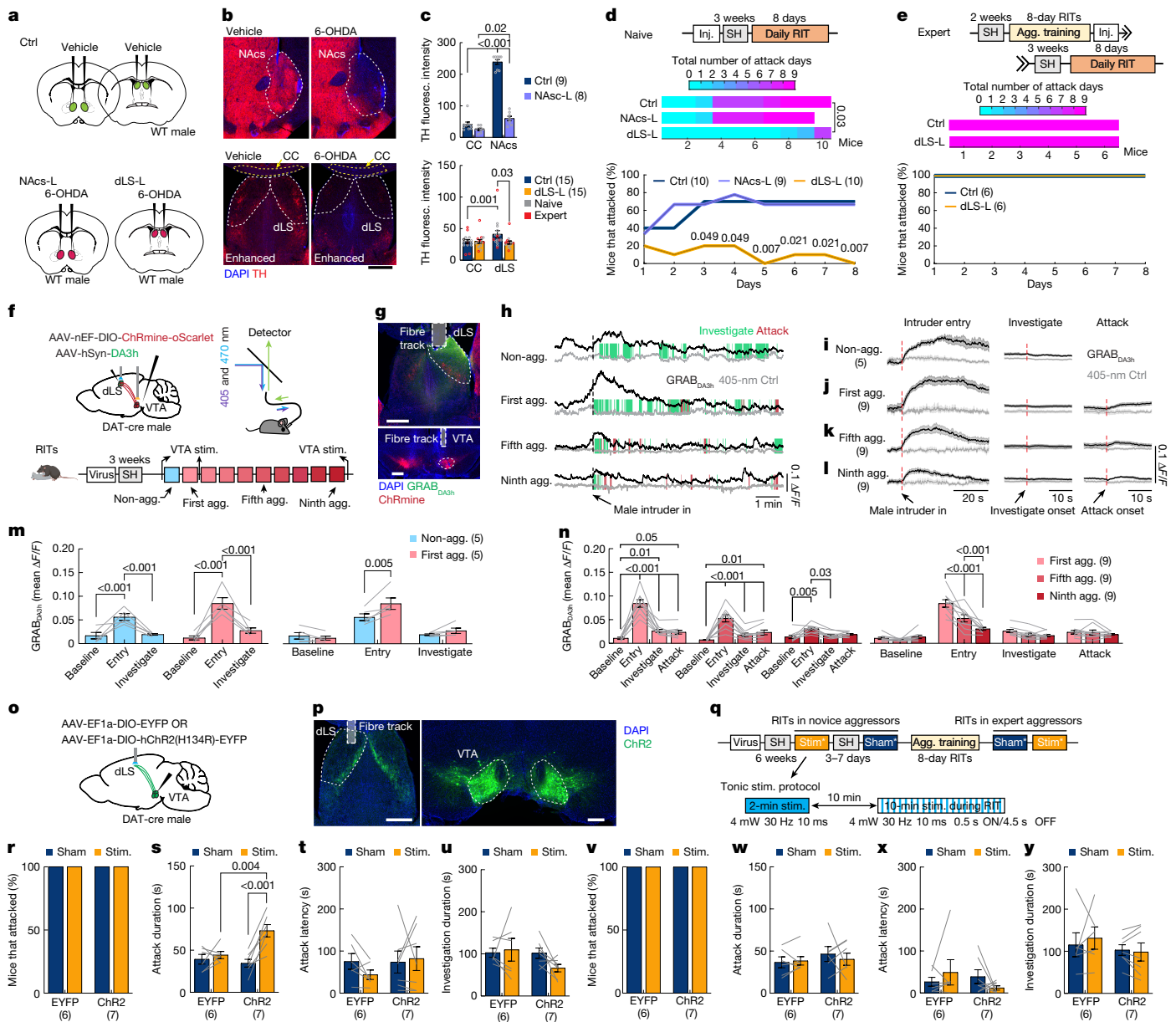


Fig. 2 | VTA^{DAT} modulates aggression in novice aggressors through projection to the dLS. **a**, Experimental design. WT, wild type. NAcS-L, NAcS-lesioned; dLS-L, dLS-lesioned. **b**, Representative histology of the NAcS (top) and the dLS (bottom) in control, NAcS-lesioned and dLS-lesioned mice. CC, corpus callosum. Scale bar, 500 μ m. **c**, Median TH fluorescence intensity in the NAcS (top), dLS (middle) and CC (control) in various groups. **d, e**, Experimental timeline (top), total attack days (middle) and percentage of mice attacking (bottom) during each test day in various groups of naive mice (**d**) and expert aggressors (**e**). *P* values in **d** (bottom) are from comparisons between control and dLS-lesioned mice. **f**, Experimental design, fibre photometry set-up and timeline to record dLS dopamine. **g**, Representative histology. Scale bars, 500 μ m. **h**, Representative $\Delta F/F$ traces of GRAB_{DASH} (black) and 405-nm control (grey) signals of the dLS during RI tests on the last non-aggressive day and on the first, fifth and ninth aggression days. Red dashed lines: male intruder introduction. **i–l**, Average per-event time histograms (PETHS) (last non-aggressive day, **i**; first (**j**), fifth (**k**) and ninth (**l**) aggression days) of GRAB_{DASH} (black) and 405-nm channel (grey) signals ($\Delta F/F$) aligned to the onset of intruder entry, investigation and attack.

Red dashed lines: behaviour onset. **m, n**, Averaged GRAB_{DASH} signals ($\Delta F/F$) during various behaviours across testing days (**m**, last non-aggressive day and first aggression day; **n**, first, fifth and ninth aggression days). **o**, Experimental design. **p**, Representative histology. Scale bars, 500 μ m. **q**, Experimental timeline and light delivery protocol. Asterisk denotes counterbalanced. **r–y**, Percentage of mice that attacked (**r, v**), attack duration (**s, w**), latency to attack (**t, x**) and investigation duration (**u, y**) of novice (**r–u**) and expert (**v–y**) aggressors on sham and light-stimulated days. White dashed rectangles in **g, p**: fibre tracks. Each line represents one mouse. Numbers in parentheses indicate numbers of mice. **d** (middle), Kruskal–Wallis test with multiple comparisons and Dunn’s correction; **e** (middle), Mann–Whitney test; **d** (bottom), **e** (bottom), Fisher’s exact tests between control and each lesion group followed by FDR correction; **m, n**, repeated-measures two-way ANOVA with multiple comparisons and Bonferroni’s or Tukey’s correction; **c, s–u, w–y**, repeated-measures two-way ANOVA with multiple comparisons and Bonferroni’s correction. See Supplementary Table 1 for statistical details. Elements (mice) in **f** were created using BioRender (<https://biorender.com>).

of VTA^{DAT} cells in naive mice (Extended Data Fig. 6a,b,d,e). Compared with the NAcc, VTA^{DAT}-activation-induced dopamine release in the dLS was smaller, and slower to reach the peak and return to baseline, although the latency to respond was similarly short in the dLS and the

NAcc (Extended Data Fig. 6d–i). Thus, dopamine releases in the dLS can be triggered rapidly by the activation of VTA^{DAT} cells, although the dopamine concentration and uptake rate are likely to be lower in the dLS than in the NAcc.

We next monitored dopamine levels in the dLS as naive mice developed into expert aggressors over repeated RI tests (Fig. 2f). When introducing the intruder and before aggression emerged, dLS dopamine increased moderately for about one minute (Fig. 2h,i), but remained unchanged during investigation (Fig. 2i,m). Dopamine increased significantly more during the intruder introduction on the first attack day than it did on the last non-aggressive day (Fig. 2h–j,m). Dopamine also increased slightly during investigation and attack (Fig. 2h,j,n). On the fifth testing day, the increase in dopamine during intruder introduction became significantly smaller than it was on the first day (Fig. 2h,j,k,n), and it continued to decline until the last testing day (Fig. 2h,l,n). On the ninth testing day, dopamine did not significantly increase during investigation and attack (Fig. 2l,n). These differences in responses probably reflect reduced VTA^{DAT} cell responses rather than a weakened VTA^{DAT} to dLS projection, because VTA^{DAT}-triggered dLS dopamine release was similar between the first and the ninth aggression days (Extended Data Fig. 6c,j–l). Furthermore, dopamine release in mice that encountered a male intruder under a cup did not change across days, suggesting that the decline in dopamine release depends on fighting experience (Extended Data Fig. 7a–g). Finally, the control 405-nm channel showed no changes in fluorescence during intruder introduction or investigation, although there was a decrease in signal during attack, possibly reflecting movement artefacts (Fig. 2h and Extended Data Fig. 7h–j). The 405-nm signal remained constant across testing days (Extended Data Fig. 7i,j).

These observations highlight three key aspects of dLS dopamine responses. First, the release of dopamine induced by the intruder is largest on the first day of aggression, supporting its potential role in aggression emergence. Second, dopamine release decreases after repeated fighting experiences, consistent with its diminished role in modulating aggression in expert aggressors. Third, compared with the NAcc, dopamine rises and falls slowly in the dLS, suggesting that it modulates the overall aggressive state as opposed to the moment-to-moment kinematics of attack bouts.

dLS dopamine promotes aggression in novices

We next asked whether artificially boosting VTA dopamine release at the dLS is sufficient to enhance inter-male aggression. Given the slow kinetics of dLS dopamine signals, we used both acute (4-mW 470-nm light, 30-ms pulses at 10 Hz for 20 s) and tonic stimulation protocols to optogenetically activate VTA^{DAT}-dLS terminals on separate days (Fig. 2o–q and Extended Data Fig. 8a,b). The latter includes a 2-min priming period (30 ms, 10 Hz) 10 min before the intruder introduction and spaced stimulation (30 ms, 10 Hz, 0.5 s on and 4.5 s off) throughout the 10-min RI test (Fig. 2q). Acute optogenetic stimulation did not change the aggressive behaviours of novice aggressors (Extended Data Fig. 8c–f). However, tonic stimulation significantly increased the total attack duration in the Chr2-expressing cells, but not in the EYFP-expressing cells, of novice aggressors, although attack latency and investigation duration did not change (Fig. 2r–u). In expert aggressors, the tonic VTA^{DAT}-dLS stimulation did not promote aggression (Fig. 2v–y). Furthermore, stimulating VTA^{DAT}-dLS lacked positive or negative valence, because Chr2 mice spent a similar time in the light chamber during the baseline and light-pairing periods in the real-time place preference (RTPP) test (Extended Data Fig. 8g,h). The VTA^{DAT}-dLS terminal stimulation did not increase FOS in VTA^{DAT} neurons, suggesting that the change in behaviour is unlikely to be due to the recruitment of other regions caused by the back propagation of action potentials (Extended Data Fig. 8i–k). In contrast to the aggression-promoting effect of VTA^{DAT}-dLS projection, tonic optogenetic activation of VTA^{DAT}-NAc terminals did not change attack duration or latency in novice aggressors, even though the stimulation increased the time spent in the light-paired chamber in the RTPP test (Extended Data Fig. 8l–s). Thus, VTA dopamine terminals at the dLS, but not at the NAc, facilitate aggression in an experience-dependent and slow manner.

Dopamine gates hippocampal flow through the dLS

We next investigated how dopamine affects dLS cell activity to modulate aggression. It was previously reported¹⁸ that 66% of recorded dLS cells showed a slow inhibitory postsynaptic potential (IPSP) when dLS dopaminergic terminals were optogenetically activated¹⁸. However, we found that only 8 out of 45 cells showed slow IPSPs, with an averaged peak amplitude of -1.88 ± 0.39 mV (Fig. 3a–f). This discrepancy might be due to dopaminergic inputs to the dLS from other regions, such as the dorsal raphe, which would be spared in our study but recruited in the previous studies using DAT-Cre: Ai32 mice^{18,39}. Indeed, applying 100 μ M dopamine hyperpolarized 30 out of 35 dLS cells (peak amplitude: -5.28 ± 0.50 mV; 30 cells) (Extended Data Fig. 9a–d). The effect of dopamine could be blocked by the D2R antagonist sulpiride (SUL, 10 μ M) or mimicked with a D2R agonist sumanirole (SUM, 1 μ M), suggesting that D2Rs mainly mediate the effects of dopamine (Extended Data Fig. 9b,d). SUL alone did not change the membrane potential significantly (Extended Data Fig. 9b,d).

The small fraction of dLS cells mildly hyperpolarized by VTA^{DAT} inputs raised doubts about the ability of this mechanism to induce robust aggression change (Fig. 2s). Given the prominent role of dopamine in synaptic plasticity⁴⁰, we asked whether VTA dopamine might also change synaptic transmission in dLS cells (Fig. 3h). After optogenetically activating VTA^{DAT} terminals for 5 min (1 ms, 30 Hz), the frequency of spontaneous inhibitory postsynaptic currents (sIPSCs), but not their amplitude, decreased in 18 out of 22 dLS cells for the recording duration (at least 5 min after the stimulation ended) (Fig. 3i,j). The change in sIPSCs could be blocked by pre-applying SUL and mimicked by SUM (Fig. 3k–m,q–t). After applying tetrodotoxin (TTX) to block spiking activity, SUM remained effective in reducing the frequency of miniature IPSCs (mIPSCs) in dLS^{Drd2} cells, indicating that the release of presynaptic inhibitory vesicles decreased (Fig. 3u–w). By contrast, the frequency and amplitude of spontaneous excitatory postsynaptic currents (sEPSCs) did not change after VTA^{DAT} terminal stimulation (Extended Data Fig. 10a–d).

The main long-range input to the dLS comes from the hippocampus and is excitatory, whereas dLS cells are overwhelmingly GABAergic and form dense local inhibitory connections⁴¹. To understand whether the dopamine-induced decrease in mIPSCs and sIPSCs reflects weakened local inhibition, we expressed Chr2 sparsely in dLS^{Drd2} cells, and voltage-clamp recorded Chr2-negative dLS cell responses to inputs from neighbouring Chr2-positive dLS^{Drd2} cells (Fig. 3x). The amplitude of light-evoked IPSCs (optical IPSCs; oIPSCs) significantly decreased and the paired-pulse ratio (PPR) of oIPSCs increased after application of SUM, suggesting that D2R activation reduced presynaptic vesicle release in dLS cells (Fig. 3y–b'). These results support the hypothesis that dLS inhibitory connections are weakened by VTA^{DAT} input.

How might decreased local inhibition in the dLS affect aggression? It has been reported that dLS cells cannot follow hippocampal stimulation of greater than 1 Hz because of a prolonged post-excitation inhibition mediated by dLS collaterals⁴². We thus asked whether dopamine can enable the propagation of hippocampal information by dampening local inhibition. Specifically, we current-clamp recorded dLS neurons while optogenetically activating CA2 and CA3 (CA2/3) terminals before and after VTA^{DAT} terminal stimulation (Fig. 4a). At the baseline, brief (0.3 ms) activation of CA2/3 terminals reliably evoked an action potential followed by a prolonged IPSP in dLS neurons (Fig. 4b). dLS cells could follow a 1-Hz hippocampal input but did not generate more than one spike when CA2/3 terminals were stimulated at 5 or 10 Hz (Fig. 4d,e). After activating VTA^{DAT} terminals for 5 min (control: 0 mW light), the post-spike IPSC amplitude significantly decreased (Fig. 4c), and spiking probability at 5-Hz and 10-Hz CA2/3 terminal stimulation significantly increased (Fig. 4d,e). SUM application also significantly reduced the post-spike IPSP amplitude (Fig. 4f–h) and increased the dLS^{Drd2} cell spike probability for 5-Hz and 10-Hz CA2/3 inputs to nearly 100% (Fig. 4i,j). Thus, dopamine can 'open the gate' for hippocampal inputs to the dLS by reducing local inhibition.

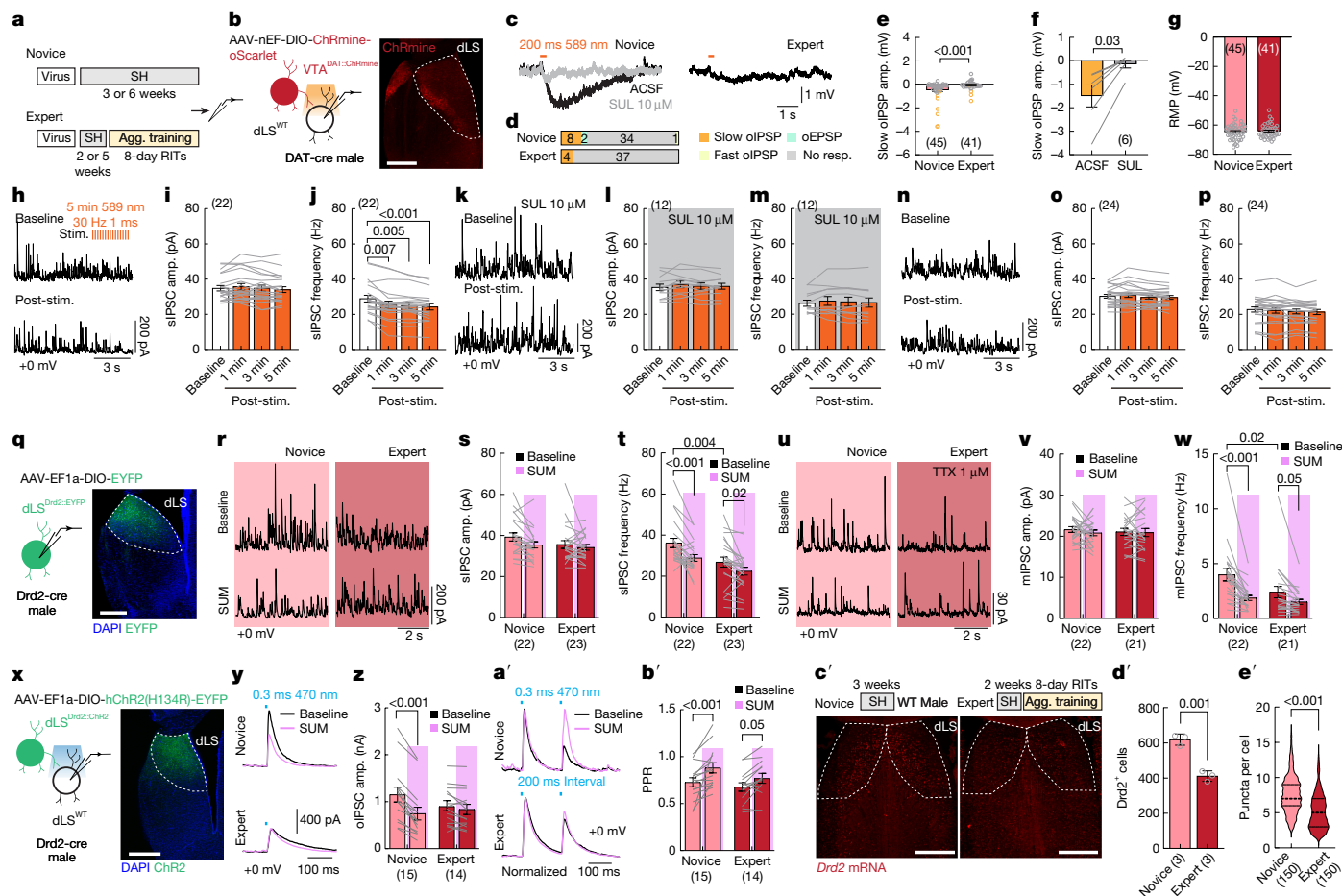


Fig. 3 | Dopamine modulation of dLS cell synaptic and cellular activities in novice and expert aggressors. **a**, Experimental timeline. **b**, Recording schematics for **c–p** and representative histology. Scale bar, 500 μ m. **c**, Representative light-evoked slow IPSPs of dLS^{WT} cells. **d**, Distribution of dLS^{WT} cell responses (**d**) and slow IPSP amplitude (**e**) after VTA^{DAT} terminal stimulation in novices and experts. No resp., no response. **f**, Light-induced slow IPSP amplitude of responsive dLS^{WT} cells in novices before and after SUL. **g**, Resting membrane potential (RMP) of dLS^{WT} cells in novices and experts. **h**, Representative sIPSC traces of a dLS^{WT} cell in a novice before (top) and after (bottom) 5-min light stimulation. **i, j**, Amplitude (**i**) and frequency (**j**) of sIPSCs before and after VTA^{DAT} terminal stimulation in novices. **k–p**, sIPSC of dLS^{WT} cells before and after VTA^{DAT} terminal stimulation in novices with SUL pre-incubation (**k–m**) and in experts (**n–p**). Plots follow conventions in **h–j**. **q**, Recording schematics for **r–w** and representative histology. Scale bar, 500 μ m. **r–t**, Representative sIPSC traces (**r**), sIPSC amplitude (**s**) and sIPSC frequency (**t**) of dLS^{Drd2} cells before (top) and after (bottom) SUM in novices and experts. **u–w**, mIPSC results. Plots follow conventions in **r–t**. **x**, Recording

schematics for **x–b'** and representative histology. Scale bar, 500 μ m. **y, a'**, Representative IPSCs evoked by one light pulse (**y**) and a pair of light pulses (**a'**) that activate neighbouring dLS^{Drd2} cells before and after SUM in novices and experts. **z, b'**, oIPSC amplitude (**z**) and PPR of oIPSCs (**b'**) before and after SUM. **c'**, Representative *Drd2* mRNA staining in the dLS in novice (left) and expert (right) aggressors. Top: experimental timeline. Scale bars, 500 μ m. **d', e'**, Number of Drd2-positive dLS cells (**d'**) and puncta per cell of 150 randomly selected Drd2-positive cells (50 cells per mouse) (**e'**) in novices and experts. Dashed line, median; dotted lines, lower and upper quartiles. Each line and circle represents one cell, except circles in **d'** that represent mice. Numbers in parentheses indicate numbers of cells or mice (**d'**). **d**, Fisher's exact tests; **e, e'**, Mann–Whitney test; **g, d'**, unpaired *t*-test; **f**, paired Wilcoxon test; **i, j, m, o**, Friedman test with multiple comparisons and Dunn's correction; **l, p**, repeated-measures one-way ANOVA with multiple comparisons and Tukey's correction; **s, t, v, w, z, b'**, repeated-measures two-way ANOVA with multiple comparisons and Bonferroni's correction. See Supplementary Table 1 for statistical details.

Lower dLS cell response to dopamine in expert mice

VTA^{DAT}–dLS projection did not modulate aggression in expert aggressors even when VTA^{DAT} terminals were artificially activated and released a similar level of dopamine to that of novice aggressors (Fig. 2v–y and Extended Data Fig. 6j–l). We thus hypothesized that dLS cells decrease their ability to sense dopamine in expert aggressors. In support of this, expert aggressors had significantly fewer Drd2-positive cells (at least two puncta per cell) in the dLS and fewer puncta per positive cell than did novice aggressors (Fig. 3c'–e'). Furthermore, dLS cells showed reduced hyperpolarization in expert aggressors to dopamine, delivered either through VTA^{DAT} terminal stimulation or by bath application (Fig. 3c–e and Extended Data Fig. 9b–d). The decreased dopamine effect was not due to changes in dLS cell resting

membrane potentials, which were comparable in experts and novices (Fig. 3g and Extended Data Fig. 9e).

Dopamine also reduced its influence on the inhibitory synaptic transmission of dLS cells in expert aggressors. VTA^{DAT} terminal stimulation did not change the frequency and amplitude of sIPSCs in dLS cells in expert aggressors (Fig. 3n–p). Direct application of a D2R agonist slightly decreased the frequencies of sIPSCs and mIPSCs in dLS^{Drd2} cells, but to a lesser extent than in novices (Fig. 3r–w). Furthermore, treatment with SUM induced no change in the amplitude of oIPSCs evoked by activating neighbouring dLS^{Drd2} cells in expert aggressors (Fig. 3x–z). The PPR of oIPSCs slightly increased after application of SUM in expert aggressors, but to a lesser extent than in novice aggressors (Fig. 3a', b'). These results collectively provide evidence that dLS cells have a weakened response to dopamine in expert aggressors.

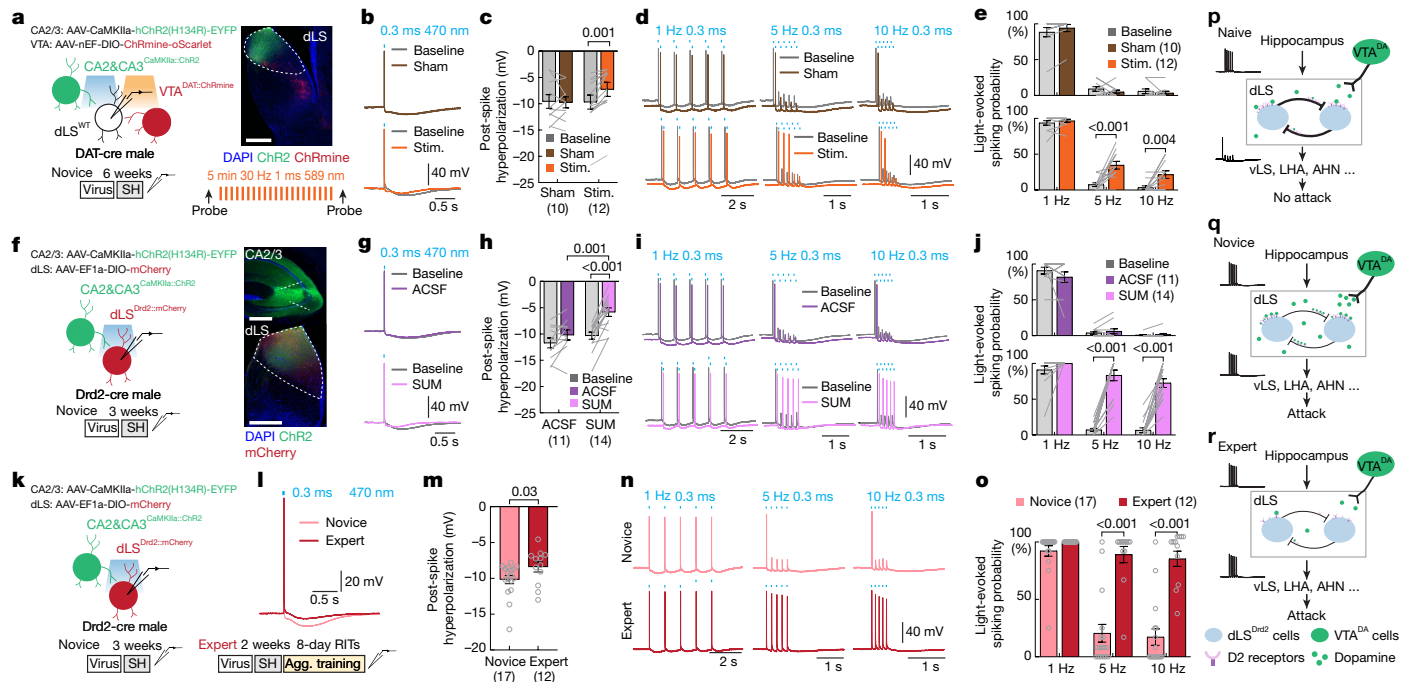


Fig. 4 | Dopamine and fighting experience enhance dLS spiking fidelity to hippocampal inputs. **a**, Recording schematics for **b–e**. Right: representative histology and light protocol to release VTA–LS dopamine. Scale bar, 500 μ m. **b,c**, Representative recording of CA2/3-input-evoked dLS^{WT} cell spiking (**b**) and average amplitude of post-spike IPSP (**c**) before and after VTA^{DAT} terminal sham (0 mW) or light stimulation. **d,e**, Representative recording (**d**) and spiking probability (**e**) of dLS^{WT} cells after 1-, 5- and 10-Hz CA2/3 inputs before and after VTA^{DAT} terminal sham or light stimulation. **f**, Recording schematics for **g–j** and representative histology. Scale bars, 500 μ m. **g,h**, Representative recording of CA2/3-input-evoked dLS^{Drd2} cell spiking (**g**) and average amplitude of post-spike IPSP (**h**) before and after ACSF or SUM. **i,j**, Representative recording trace (**i**) and spiking probability (**j**) of dLS^{Drd2} cells after 1-, 5- and 10-Hz CA2/3 inputs before and after ACSF or SUM. **k**, Recording schematics for **l–o**. **l,m**, Representative recording of CA2/3-input-evoked dLS^{Drd2} cell spiking (**l**) and average amplitude of the post-spike IPSP (**m**) in novices and experts.

n,o, Representative recording (**n**) and spiking probability (**o**) of dLS^{Drd2} cells after 1-, 5- and 10-Hz CA2/3 terminal stimulation in novices and experts. **p–r**, dLS cells in naive mice form strong mutual inhibition, blocking excitatory hippocampal inputs from reaching downstream areas and preventing attack initiation (**p**). Over male–male interaction, the increased dLS dopamine release weakens dLS local inhibition through D2R, allowing hippocampal information to pass and facilitate aggression (**q**). Over repeated fighting, dLS local inhibition weakens, enabling hippocampal information to pass without the assistance of dopamine (**r**). As the role of dopamine diminishes, dopamine release during male–male interaction and dLS cell responses to dopamine decrease. Each circle and line represents one cell. Numbers inside parentheses indicate recorded cell numbers. **c,e,h,j,o**, repeated-measures two-way ANOVA with multiple comparisons and Bonferroni’s correction; **m**, Mann–Whitney test. See Supplementary Table 1 for statistical details.

Reduced intra-dLS inhibition in expert mice

Why does dLS dopamine become nonessential for aggression in experts? If dopamine opens the gate for hippocampal inputs, we wonder whether the dLS gate is already open in expert aggressors without dopamine. Consistent with this hypothesis, the frequencies of sIPSCs and mIPSCs in dLS^{Drd2} cells were significantly lower in experts than in novice aggressors (Fig. 3t,w). Notably, D2R agonist reduced the s/mIPSC frequency in novices to a level similar to the baseline level of expert aggressors (Fig. 3r,t,u,w). In contrast to the IPSCs, the frequencies of sEPSCs and mEPSCs in dLS cells did not differ between novice and expert aggressors (Extended Data Fig. 10e,f,h,i,k). However, the amplitude of sEPSCs, but not mEPSCs, decreased significantly in expert aggressors (Extended Data Fig. 10g,j). This decrease might reflect reduced spiking-induced EPSCs, because the sEPSC amplitude showed a multimodal distribution in novice aggressors, with clusters of 1 \times , 2 \times and 3 \times mEPSC amplitude (Extended Data Fig. 10g,j). In expert aggressors, the sEPSC amplitudes of nearly all cells were similar to those of mEPSCs (Extended Data Fig. 10g,j). Thus, the spontaneous firing of dLS upstream excitatory cells might decrease in expert aggressors.

Finally, the amplitude of the slow post-spike IPSP in dLS cells from expert aggressors was significantly lower than that in novice aggressors (Fig. 4k–m). Crucially, when we stimulated the CA2/3 terminals at 5 Hz and 10 Hz, the dLS cells in expert aggressors spiked with nearly 100% reliability—markedly different from the single-spike response pattern

that was observed in novice aggressors (Fig. 4n–o). These results suggest that the dLS local inhibitory network is weakened in expert aggressors, which enables hippocampal information to flow even without the assistance of dopamine.

Discussion

Decades of gain- and loss-of-function experiments revealed that the lateral septum has a crucial role in modulating aggression^{24,43–45}. Circuit studies have provided further details: whereas the vLS suppresses aggression through its projection to the medial hypothalamus, the dLS enhances aggression by inhibiting the vLS^{23,24}. Here, we found that the strong intra-dLS inhibitory network in naive mice prevents dLS cells from responding to the excitatory hippocampal inputs, which presumably will limit the influence of the hippocampus on downstream circuits (Fig. 4p). The dopamine projection from the VTA to the dLS dampens local inhibition in naive mice, which enables the dLS cells to respond to excitatory inputs with greater fidelity, and ultimately facilitates attack initiation (Fig. 4q). When we impaired the dopaminergic input from the VTA to the dLS by inhibiting VTA^{DAT} cells, blocking VTA dopamine synthesis or depleting dLS dopaminergic inputs, aggression did not increase in naive male mice, highlighting the crucial role of the VTA–dLS dopamine circuit in the development of aggression in adult males. Notably, as males become experienced in fighting, the role of dLS dopamine in aggression diminishes. In expert aggressors, suppressing

VTA^{DAT} cell activity, blocking VTA dopamine synthesis or ablating dLS dopaminergic inputs caused no deficit in aggression. The reduced role of dopamine in the dLS in expert aggressors could be explained by changes in dLS local inhibition. After repeated winning, inhibitory connections among dLS cells weaken, which enables hippocampal inputs to recruit dLS circuits reliably without the assistance of dopamine (Fig. 4r). As the need for dopamine diminishes, the liberation of dopamine in the dLS during male encounters and the ability of dLS cells to sense dopamine also reduce. We should note that our study did not directly investigate the circuit downstream of the dLS. Although the dLS could exert its effects on aggression through the previously identified dLS–vLS–VMHvl circuit^{23,24}, it might also modulate aggression through its projections to other aggression-related regions, such as the lateral hypothalamus and the anterior hypothalamus^{46,47} (Fig. 4p–r). Beyond the dLS, the medial hypothalamic regions that directly drive attack also undergo extensive synaptic and cellular plasticity with repeated fighting experience^{29,48–50}. These changes are likely to help the aggression cells overcome inhibition from the vLS or other regions more readily and reduce their reliance on dLS cells in attack initiation.

Our study reveals that VTA dopaminergic neurons have an experience-dependent and sexually dimorphic role in modulating aggression, by facilitating the output of the dLS (Supplementary Note 1). These findings suggest that early interventions that target dopamine receptors could be used to prevent the escalation of aggression, and highlight the potential need for sex-specific strategies to manage and treat aggression.

Online content

Any methods, additional references, Nature Portfolio reporting summaries, source data, extended data, supplementary information, acknowledgements, peer review information; details of author contributions and competing interests; and statements of data and code availability are available at <https://doi.org/10.1038/s41586-024-08459-w>.

- Lischinsky, J. E. & Lin, D. Neural mechanisms of aggression across species. *Nat. Neurosci.* **23**, 1317–1328 (2020).
- de Almeida, R. M., Ferrari, P. F., Parmigiani, S. & Miczek, K. A. Escalated aggressive behavior: dopamine, serotonin and GABA. *Eur. J. Pharmacol.* **526**, 51–64 (2005).
- Yamaguchi, T. & Lin, D. Functions of medial hypothalamic and mesolimbic dopamine circuitries in aggression. *Curr. Opin. Behav. Sci.* **24**, 104–112 (2018).
- Citrome, L. & Volavka, J. Psychopharmacology of violence: Part I: Assessment and acute treatment. *Psychiatr. Ann.* **27**, 691–695 (1997).
- Yudofsky, S. C., Silver, J. M. & Schneider, S. E. Pharmacologic treatment of aggression. *Psychiatr. Ann.* **17**, 397–407 (1987).
- Buckley, P. F. The role of typical and atypical antipsychotic medications in the management of agitation and aggression. *J. Clin. Psychiatry* **60**, 52–60 (1999).
- O'Malley, K. Y., Hart, C. L., Casey, S. & Downey, L. A. Methamphetamine, amphetamine, and aggression in humans: a systematic review of drug administration studies. *Neurosci. Biobehav. Rev.* **141**, 104805 (2022).
- Miczek, K. A. Intraspecific aggression in rats: effects of *d*-amphetamine and chlordiazepoxide. *Psychopharmacologia* **39**, 275–301 (1974).
- Krsiak, M. et al. Drug effects on attack defense and escape in mice. *Pharmacol. Biochem. Behav.* **14**, 47–52 (1981).
- Miczek, K. A., Fish, E. W., De Bold, J. F. & De Almeida, R. M. Social and neural determinants of aggressive behavior: pharmacotherapeutic targets at serotonin, dopamine and γ -aminobutyric acid systems. *Psychopharmacology* **163**, 434–458 (2002).
- McMillen, B. A., DaVanzo, E. A., Song, A. H., Scott, S. M. & Rodriguez, M. E. Effects of classical and atypical antipsychotic drugs on isolation-induced aggression in male mice. *Eur. J. Pharmacol.* **160**, 149–153 (1989).
- Aguilar, M. A., Miñarro, J., Pérez-Iranzo, N. & Simón, V. M. Behavioral profile of raclopride in agonistic encounters between male mice. *Pharmacol. Biochem. Behav.* **47**, 753–756 (1994).
- Tidey, J. W. & Miczek, K. A. Effects of SKF 38393 and quinpirole on aggressive, motor and schedule-controlled behaviors in mice. *Behav. Pharmacol.* **3**, 553–565 (1992).
- Kolla, N. J. & Bortolato, M. The role of monoamine oxidase A in the neurobiology of aggressive, antisocial, and violent behavior: a tale of mice and men. *Prog. Neurobiol.* **194**, 101875 (2020).
- Qayyum, A. et al. The role of the catechol-O-methyltransferase (COMT) GeneVal158Met in aggressive behavior, a review of genetic studies. *Curr. Neuropharmacol.* **13**, 802–814 (2015).
- Rodríguez, R. M., Chu, R., Caron, M. G. & Wetsel, W. C. Aberrant responses in social interaction of dopamine transporter knockout mice. *Behav. Brain Res.* **148**, 185–198 (2004).

- Gogos, J. A. et al. Catechol-O-methyltransferase-deficient mice exhibit sexually dimorphic changes in catecholamine levels and behavior. *Proc. Natl. Acad. Sci. USA* **95**, 9991–9996 (1998).
- Mahadevia, D. et al. Dopamine promotes aggression in mice via ventral tegmental area to lateral septum projections. *Nat. Commun.* **12**, 6796 (2021).
- Yu, Q. et al. Dopamine and serotonin signaling during two sensitive developmental periods differentially impact adult aggressive and affective behaviors in mice. *Mol. Psychiatry* **19**, 688–698 (2014).
- Golden, S. A. et al. Basal forebrain projections to the lateral habenula modulate aggression reward. *Nature* **534**, 688–692 (2016).
- Flanigan, M., Aleyasin, H., Takahashi, A., Golden, S. A. & Russo, S. J. An emerging role for the lateral habenula in aggressive behavior. *Pharmacol. Biochem. Behav.* **162**, 79–86 (2017).
- Poulin, J. F. et al. Mapping projections of molecularly defined dopamine neuron subtypes using intersectional genetic approaches. *Nat. Neurosci.* **21**, 1260–1271 (2018).
- Leroy, F. et al. A circuit from hippocampal CA2 to lateral septum disinhibits social aggression. *Nature* **564**, 213–218 (2018).
- Wong, L. C. et al. Effective modulation of male aggression through lateral septum to medial hypothalamus projection. *Curr. Biol.* **26**, 593–604 (2016).
- Lin, D. et al. Functional identification of an aggression locus in the mouse hypothalamus. *Nature* **470**, 221–226 (2011).
- Armbruster, B. N., Li, X., Pausch, M. H., Herlitze, S. & Roth, B. L. Evolving the lock to fit the key to create a family of G protein-coupled receptors potentially activated by an inert ligand. *Proc. Natl. Acad. Sci. USA* **104**, 5163–5168 (2007).
- Kudryavtseva, N. N., Lipina, T. V. & Koryakina, L. A. Effects of haloperidol on communicative and aggressive behavior in male mice with different experiences of aggression. *Pharmacol. Biochem. Behav.* **63**, 229–236 (1999).
- Thompson, K. J. et al. DREADD agonist 21 is an effective agonist for muscarinic-based DREADDs in vitro and in vivo. *ACS Pharmacol. Transl. Sci.* **1**, 61–72 (2018).
- Yan, R. et al. The multi-stage plasticity in the aggression circuit underlying the winner effect. *Cell* **187**, 6785–6803 (2024).
- Lee, H. et al. Scalable control of mounting and attack by *Esr1*⁺ neurons in the ventromedial hypothalamus. *Nature* **509**, 627–632 (2014).
- Hashikawa, K. et al. *Esr1*⁺ cells in the ventromedial hypothalamus control female aggression. *Nat. Neurosci.* **20**, 1580–1590 (2017).
- Yang, T. et al. Social control of hypothalamus-mediated male aggression. *Neuron* **95**, 955–970 (2017).
- Hashikawa, K., Hashikawa, Y., Lischinsky, J. & Lin, D. The neural mechanisms of sexually dimorphic aggressive behaviors. *Trends Genet.* **34**, 755–776 (2018).
- Hunker, A. C. et al. Conditional single vector CRISPR/SaCas9 viruses for efficient mutagenesis in the adult mouse nervous system. *Cell Rep.* **30**, 4303–4316 (2020).
- da Silva, J. A., Tecuapetla, F., Paixão, V. & Costa, R. M. Dopamine neuron activity before action initiation gates and invigorates future movements. *Nature* **554**, 244–248 (2018).
- Golden, S. A. et al. Nucleus accumbens *Drd1*-expressing neurons control aggression self-administration and aggression seeking in mice. *J. Neurosci.* **39**, 2482–2496 (2019).
- Aleyasin, H. et al. Cell-type-specific role of Δ FosB in nucleus accumbens in modulating intermale aggression. *J. Neurosci.* **38**, 5913–5924 (2018).
- Zhuo, Y. et al. Improved green and red GRAB sensors for monitoring dopaminergic activity in vivo. *Nat. Methods* **21**, 680–691 (2024).
- Cardozo Pinto, D. F. et al. Characterization of transgenic mouse models targeting neuromodulatory systems reveals organizational principles of the dorsal raphe. *Nat. Commun.* **10**, 4633 (2019).
- Tritsch, N. X. & Sabatini, B. L. Dopaminergic modulation of synaptic transmission in cortex and striatum. *Neuron* **76**, 33–50 (2012).
- Besnard, A. & Leroy, F. Top-down regulation of motivated behaviors via lateral septum sub-circuits. *Mol. Psychiatry* **27**, 3119–3128 (2022).
- Liu, J. J., Tsien, R. W. & Pang, Z. P. Hypothalamic melanin-concentrating hormone regulates hippocampus-dorsolateral septum activity. *Nat. Neurosci.* **25**, 61–71 (2022).
- Albert, D. J. & Chew, G. L. The septal forebrain and the inhibitory modulation of attack and defense in the rat. A review. *Behav. Neural Biol.* **30**, 357–388 (1980).
- Slotnick, B. M., McMullen, M. F. & Fleischer, S. Changes in emotionality following destruction of the septal area in albino mice. *Brain Behav. Evol.* **8**, 241–252 (1973).
- Potegal, M., Blau, A. & Glusman, M. Effects of anteroventral septal lesions on intraspecific aggression in male hamsters. *Physiol. Behav.* **26**, 407–412 (1981).
- Haller, J. The role of the lateral hypothalamus in violent intraspecific aggression—the glucocorticoid deficit hypothesis. *Front. Syst. Neurosci.* **12**, 26 (2018).
- Ferris, C. F. et al. Vasopressin/serotonin interactions in the anterior hypothalamus control aggressive behavior in golden hamsters. *J. Neurosci.* **17**, 4331–4340 (1997).
- Stagkourakis, S., Spigolon, G., Liu, G. & Anderson, D. J. Experience-dependent plasticity in an innate social behavior is mediated by hypothalamic LTP. *Proc. Natl. Acad. Sci. USA* **117**, 25789–25799 (2020).
- Falkner, A. L., Grosenick, L., Davidson, T. J., Deisseroth, K. & Lin, D. Hypothalamic control of male aggression-seeking behavior. *Nat. Neurosci.* **19**, 596–604 (2016).
- Stagkourakis, S. et al. A neural network for intermale aggression to establish social hierarchy. *Nat. Neurosci.* **21**, 834–842 (2018).

Publisher's note Springer Nature remains neutral with regard to jurisdictional claims in published maps and institutional affiliations.

Springer Nature or its licensor (e.g. a society or other partner) holds exclusive rights to this article under a publishing agreement with the author(s) or other rightsholder(s); author self-archiving of the accepted manuscript version of this article is solely governed by the terms of such publishing agreement and applicable law.

© The Author(s), under exclusive licence to Springer Nature Limited 2025

Methods

Mice

All procedures were approved by the NYULMC Institutional Animal Care and Use Committee (IACUC) in compliance with the National Institutes of Health (NIH) Guidelines for the Care and Use of Laboratory Animals. Mice were housed under a 12-h light–dark cycle (dark cycle; 10:00 to 22:00 or 18:30 to 06:30), with food and water available ad libitum. Room temperature was maintained at 20–22 °C and humidity at 30–70%, with a daily average of approximately 45%. Test mice were adult DAT-Cre (Jackson, 006660), *Drd2*-Cre (MMRRC_032108-UCD), *Esr1*-2A-Cre (Jackson, 017911) and wild-type C57BL/6N (Charles River, 027) mice. They were between 8 and 20 weeks old at the time of behaviour testing or recording. Intruder mice in the inter-male RI tests were adult BC (older than 8 weeks) male mice. During each RI test, the intruder was randomly picked from a group of 20–30 mice, housed 4–5 mice per cage. For the male–female RI test, adult C57BL/6N or BC (older than 8 weeks) female mice were used. For the female aggression test, juvenile C57BL/6N (approximately 21–28 days old) male mice were used. All intruder mice were originally purchased from Charles River and then bred in-house. They were group-housed until adulthood. Females were considered receptive if an experienced male could mount and intromit the female within three attempts. After surgery, all male test mice were single-housed, and female test mice were paired with adult male mice until the females became visibly pregnant. Mice were randomly assigned to control and test groups. All experiments were performed during the dark cycle of the mice.

Viruses

AAV8-hSyn-DIO-hM4Di-mCherry (1.8×10^{13} vg ml⁻¹, Addgene, 44362-AAV8), AAV5-hSyn-DIO-hM3Dq-mCherry (2.0×10^{13} vg ml⁻¹, Addgene, 44361-AAV5), AAV2-hSyn-DIO-hM3D(Gq)-mCherry (2.6×10^{13} vg ml⁻¹, Addgene, 44361-AAV2) and AAV8-nEF-Con/Foff-ChRmine-oScarlet (2.3×10^{13} vg ml⁻¹, Addgene, 137161-AAV8) were purchased from Addgene. AAV5-EF1a-DIO-EYFP (3.5×10^{12} vg ml⁻¹, UNC, AV4310), AAV5-EF1a-DIO-hChR2(H134R)-EYFP (4.0×10^{12} vg ml⁻¹, UNC, AV4313), AAV5-CaMKIIa-hChR2(H134R)-EYFP (6.2×10^{12} vg ml⁻¹, UNC, AV4316), AAV5-EF1a-DIO-mCherry (5.1×10^{12} vg ml⁻¹, UNC, AV4311) and AAV2-hSyn-DIO-mCherry (5.6×10^{12} vg ml⁻¹, UNC, AV4753) were purchased from University of North Carolina vector core. AAV-hSyn-DA3h (5.85×10^{12} vg ml⁻¹, BrainVTA, PT4721) was purchased from BrainVTA. AAV1-CMV-FLEX-EGFP-KASH, AAV1-CMV-FLEX-SaCas9-U6-sgTH and AAV1-CMV-FLEX-SaCas9-U6-sgRosa26 were provided by L. Zweifel.

Stereotaxic surgery

Mice were anaesthetized with 1–1.5% isoflurane and placed in a stereotaxic frame (Kopf Instruments, model 1900). Viruses or chemicals were delivered into the brains through a glass capillary using a nanoinjector (World Precision Instruments, Nanoliter 2000) at a speed of 20 nl min⁻¹. Stereotaxic injection coordinates were based on the Paxinos and Franklin mouse brain atlas⁵¹.

For VTA^{DAT} chemogenetic manipulation²⁶, 140 nl per side of AAV8-hSyn-DIO-hM4Di-mCherry, AAV5-hSyn-DIO-hM3Dq-mCherry or AAV2-hSyn-DIO-mCherry (as a control) was injected bilaterally into the VTA (Bregma coordinates: AP: -3.10 mm, ML: ±0.5 mm, DV: -4.50 mm) of heterozygous DAT-Cre mice. For VMHvl manipulation, we bilaterally injected 80 nl per side of AAV2-hSyn-DIO-hM3D(Gq)-mCherry into the VMHvl (AP: -1.70 mm, ML: ±0.75 mm, DV: -5.80 mm) of heterozygous *Esr1*-2A-Cre male mice.

For TH mutagenesis³⁴, we mixed AAV1-CMV-FLEX-EGFP-KASH with either AAV1-CMV-FLEX-SaCas9-U6-sgTH or AAV1-CMV-FLEX-SaCas9-U6-sgRosa26 at 1:2 ratio and then bilaterally injected 240 nl per side of the mixed viruses into the VTA (AP: -3.10 mm, ML: ±0.5 mm, DV: -4.50 mm) of heterozygous DAT-Cre mice.

For dopamine terminal ablation, we administered 25 mg kg⁻¹ desipramine (Thermo Fisher Scientific, 30-675-0) intraperitoneally 30 min

before 6-OHDA injection to protect noradrenaline terminals and then bilaterally injected 60 nl per side of 6-OHDA solution into either the NAc (AP: 0.98 mm, ML: ±0.5 mm, DV: -4.60 mm) or the dLS (AP: 0.14 mm, ML: ±0.4 mm, DV: -2.60 mm) of wild-type C57BL/6N male mice. For the control mice, we injected the vehicle into both the dLS and the NAc. The 6-OHDA solution was prepared right before the injection by dissolving 15 mg of 6-OHDA (Sigma-Aldrich, H4381) in 1 ml 0.2% ascorbic acid.

For dopamine recording³⁸, we injected 100 nl AAV-hSyn-DA3h into the dLS unilaterally (AP: 0.14 mm, ML: ±0.4 mm, DV: -2.60 mm) and 140 nl per side of AAV8-nEF-Con/Foff-ChRmine-oScarlet into the VTA bilaterally (AP: -3.10 mm, ML: ±0.5 mm, DV: -4.50 mm) of heterozygous DAT-Cre male mice for RI tests. We then implanted two custom-made optic fibre assemblies (Thorlabs, FT400EMT and SFLC440) approximately 300 µm above the injection sites in the dLS and VTA on the same hemisphere. These fibres were then secured in place using dental cement (C&B Metabond, S380). We also injected 100 nl of AAV-hSyn-DA3h into the NAcc unilaterally (AP: 0.14 mm, ML: ±1.20 mm, DV: -4.60 mm) and 140 nl per side of AAV8-nEF-Con/Foff-ChRmine-oScarlet into the VTA bilaterally (AP: -3.10 mm, ML: ±0.5 mm, DV: -4.50 mm) of heterozygous DAT-Cre male mice, and then implanted the same fibre assemblies above the injection sites. For dopamine recording during non-aggressive social interaction tests, we injected 100 nl of AAV-hSyn-DA3h into the dLS unilaterally (AP: 0.14 mm, ML: ±0.4 mm, DV: -2.60 mm) of wild-type male mice and then implanted the same fibre assemblies above the injection sites.

For VTA^{DAT}-dLS and terminal optogenetic activation⁵², we injected 140 nl per side of either AAV5-EF1a-DIO-hChR2(H134R)-EYFP or AAV5-EF1a-DIO-EYFP into the VTA bilaterally (AP: -3.10 mm, ML: ±0.5 mm, DV: -4.50 mm) of heterozygous DAT-Cre male mice. After virus injection, a custom-made optic fibre assembly (Thorlabs, FT200EMT and CFLC230) was implanted unilaterally approximately 300 µm above the dLS (AP: 0.14 mm, ML: ±0.4 mm, DV: -2.60 mm) and secured using dental cement (C&B Metabond, S380). For VTA^{DAT}-NAc terminal optogenetic activation, we injected 140 nl per side of AAV5-EF1a-DIO-hChR2(H134R)-EYFP into the VTA bilaterally (AP: -3.10 mm, ML: ±0.5 mm, DV: -4.50 mm) of heterozygous DAT-Cre male mice. After virus injection, two custom-made optic fibre assemblies (Thorlabs, FT200EMT and CFLC230) were implanted bilaterally above the injection sites.

For slice recordings, to stimulate VTA^{DAT} terminals, we injected 140 nl per side of AAV8-nEF-Con/Foff-ChRmine-oScarlet bilaterally into the VTA (AP: -3.10 mm, ML: ±0.5 mm, DV: -4.50 mm) of heterozygous DAT-Cre male mice. To label dLS^{Drd2} cells, we injected 120 nl per side of AAV5-EF1a-DIO-EYFP bilaterally into the dLS (AP: 0.14 mm, ML: ±0.4 mm, DV: -2.60 mm) of *Drd2*-Cre male mice. To investigate the dLS local network, we diluted the AAV5-EF1a-DIO-hChR2(H134R)-EYFP to a final titre of 1×10^{12} gc ml⁻¹, and injected 60 nl per side of the diluted virus into dLS bilaterally (AP: 0.14 mm, ML: ±0.4 mm, DV: -2.60 mm) of *Drd2*-Cre male mice. To examine the dLS^{Drd2} cell responses to the excitatory inputs from CA2/3, we injected 160 nl per side of AAV5-CaMKIIa-hChR2(H134R)-EYFP into CA2/3 bilaterally (AP: -1.70 mm, ML: ±2.05 mm, DV: -1.80 mm) and 120 nl per side of AAV5-EF1a-DIO-mCherry into the dLS bilaterally (AP: 0.14 mm, ML: ±0.4 mm, DV: -2.60 mm) of *Drd2*-Cre male mice. To investigate the effect of VTA^{DAT} terminal activation on dLS cell responses to the excitatory inputs from CA2/3, we injected 160 nl per side of AAV5-CaMKIIa-hChR2(H134R)-EYFP into the CA2/3 bilaterally (AP: -1.70 mm, ML: ±2.05 mm, DV: -1.80 mm) and 140 nl per side of AAV8-nEF-Con/Foff-ChRmine-oScarlet into the VTA bilaterally (AP: -3.10 mm, ML: ±0.5 mm, DV: -4.50 mm) of heterozygous DAT-Cre male mice.

Identification of novice mice

On the basis of our previous experience, the male mouse that weighs the least in a cage of four or five mice is less likely to become aggressive

Article

after single housing. Therefore, we measured the weight of all mice and excluded the lowest-weight mouse in a cage before surgery. Three (for cell body manipulation) or six (for terminal manipulation) weeks after surgery, the test mice went through the 10-min RI test for up to three days. During each RI test, a non-aggressive group-housed BC male intruder was introduced. Once the test mouse initiated attack and won the fight, the intruder was removed. After the test mouse won one RI test, it was considered a novice aggressor and used for subsequent experiments. Mice that did not display any aggression in all three RI tests were excluded. Naive mice used in TH mutagenesis and 6-OHDA lesion experiments were not subjected to any pre-screening procedures.

Pharmacogenetic manipulation

To chemogenetically manipulate VTA^{DAT} and VMHv^{Esr1} cell activity in male aggressors, we used the RI tests three weeks after surgery to identify novice aggressors. During this process, the test mice underwent a daily 10-min RI test against a non-aggressive group-housed BC male intruder for up to three days. Once the test mouse attacked and won one RI test, they were considered novice aggressors. We then divided the novice aggressors into two groups. One group received i.p. injection of saline, and the other group received 1 mg kg⁻¹ C21 (Tocris, 5548), a specific ligand of hM4Di^{28,53}. Thirty minutes after injections, we assessed the aggression level of the test mice by introducing a BC male intruder into the test mouse's home cage for 10 min. After the aggression test, we tested the sexual behaviour of the mouse by introducing a receptive female into the test mouse's home cage. The female's sexual receptivity was predetermined by introducing the female into the cage of a sexually experienced male. If the female allowed the male to mount and intromit, the female was deemed receptive. After the aggression and sexual behaviour tests, for the VTA^{DAT} groups, we also examined the locomotion of the test mouse by placing it in a large open arena (45.7 × 45.7 × 38.1 cm, acrylic) for 10 min. After completing all the tests, the mouse was singly housed for three to seven days without disturbance. We then repeated the tests after switching the C21 and saline treatments. The mice then underwent daily RI tests for another eight days with male BC intruders to become expert aggressors. We then i.p. injected C21 and saline again on separate days and performed aggression tests with BC male intruders, sexual behaviour tests with receptive females and locomotion tests in the open arena (only for VTA^{DAT} groups).

For chemogenetic activation of VTA^{DAT} cells in virgin females, three weeks after virus injection, we examined the vaginal smears and selected females that were in dioestrus. The test females were then i.p. injected with either saline or 1 mg kg⁻¹ C21 on separate dioestrus days and tested with a male juvenile intruder (approximately 21–28 days old) for 10 min 30 min later. Immediately after the RI tests, locomotion was evaluated in a large open arena for 10 min. For chemogenetic activation or inhibition of VTA^{DAT} cells in lactating females, test females were paired with male C57 mice until they were visibly pregnant. Two days after pup delivery, we identified females showing robust maternal aggression by introducing a juvenile male mouse (approximately 21–28 days old) into the female's home cage for 10 min. Aggressive females were then i.p. injected with either saline or 1 mg kg⁻¹ C21 on separate days and tested with a male juvenile intruder for 10 min 30 min later. Immediately after the RI tests, locomotion was evaluated in a large open arena for 10 min.

CRISPR–Cas9-mediated TH mutagenesis

To induce TH mutagenesis of VTA^{DAT} cells in naive mice, we injected viruses expressing Cre-dependent SaCas9-sgTH or SaCas9-sgRosa26 into group-housed DAT-Cre male mice. The mice were singly housed after surgery. To induce TH mutagenesis in expert mice, we single-housed naive DAT-Cre male mice for two weeks, then subjected the mice to daily RI tests with BC male intruders until the mice showed eight consecutive wins. Mice that did not attack in the first three days of RI tests or did not attack consistently across days were excluded. We then injected either SaCas9-sgTH or SaCas9-sgRosa26 virus into the

VTA of these experienced aggressors. Four weeks after virus injection, we subjected all test mice to daily 10-min RI tests with group-housed BC male intruders for eight consecutive days. After completing all RI tests with males, we tested the test mouse's sexual behaviour by introducing a receptive female for 10 min. The mice were then tested for locomotion in an open arena for 10 min.

6-OHDA lesion

To examine the role of dopamine signalling in the emergence of aggression, group-housed C57BL/6N naive male mice were injected with 6-OHDA into the NAc, 6-OHDA into the dLS and vehicle into both the NAc and the dLS. In addition, we injected 6-OHDA or vehicle into the dLS of expert aggressors. Expert aggressors were generated by subjecting single-housed naive C57BL/6N male mice to daily RI tests with BC male intruders. Mice that won eight days in a row were considered expert aggressors. All mice were singly housed after 6-OHDA injection. Four weeks after 6-OHDA injection, we subjected all mice to daily 10-min RI tests with BC male intruders for eight consecutive days.

Optogenetic activation

To understand the effect of optogenetic activation of VTA^{DAT}-dLS and VTA^{DAT}-NAc terminals, we first identified novice aggressors using RI tests six weeks after virus injection. One day after the screening and on the first testing day, half of the mice received 2 min, 4 mW, 30 Hz, 10 ms and 470 nm light stimulation 10 min before intruder introduction and 4 mW, 30 Hz, 10 ms and 0.5 s light train every 5 s throughout the 10-min RI test. The other half of the mice received no light stimulation before or during the RI test. Three to seven days after the first tests, we repeated the RI tests with the light condition switched for each mouse.

After examining the effect of tonic light stimulation of VTA^{DAT}-dLS terminals on aggression, we tested the effect of the acute light stimulation on aggression on a separate day. During the test, we delivered 4 mW, 30 Hz, 10 ms, 20 s and 470 nm light stimulation or sham (0 mW) light when the test mouse investigated the intruder. The light and sham light were each delivered four times in a randomized order. The attack latency was calculated as the time elapsed from the light onset to the first attack. If no attack occurred during the 20-s stimulation, the latency was considered 20 s. The attack probability was calculated as the proportion of trials in which the test mouse attacked.

Then, the test mice underwent daily RI tests with male BC intruders for seven consecutive days and became expert aggressors. We then tested the effect of tonic light stimulation on aggressive behaviours during the 10-min RI tests using the same light protocol as for the novice aggressors. The light and no-light conditions were tested on separate days, and the testing order was counterbalanced across mice.

The RTPP test was performed on the same day as the RI test with acute light stimulation for the VTA^{DAT}-dLS group and on a separate day for the VTA^{DAT}-NAc group. The RTPP arena contains two equal-sized chambers (13 cm × 16 cm × 25 cm each, acrylic). The test mice were first habituated in the arena for 10 min. Then, we recorded behaviour for 10 min without stimulation to establish a baseline. Finally, we manually turned on the light (4 mW, 30 Hz, 10 ms) whenever the mice entered a predetermined chamber. The mice's body centre positions were tracked using DeepLabCut⁵⁴.

To evaluate whether the light activation of VTA^{DAT}-dLS terminals results in any back propagation of action potentials, we performed the tonic light activation as described above in a group of naive male mice without the presence of a male intruder. Seventy minutes later, the mice were perfused with phosphate-buffered saline (PBS) and 4% paraformaldehyde (PFA), and their brains were collected for quantifying FOS in the VTA.

Fibre photometry

The GRAB_{DA3h} fluorescence signals were recorded using fibre photometry^{55,56}. In brief, bandpass-filtered 400-Hz-modulated 470-nm

LED light (Semrock, FF02-472/30-25) and 317-Hz-modulated 405-nm LED light (Semrock, FBH405-10) were combined and delivered to the brain through the implanted optic fibre. The emission light was passed through the same optic fibre, filtered (Semrock, FF01-535/505), detected by a Femtowatt Silicon Photoreceiver (Newport, 2151) and recorded using a TDT real-time processor (Newport, RZ5). The envelopes of 400-Hz- and 317-Hz-modulated photocurrents were extracted as dopamine-dependent and dopamine-independent fluorescence signals using a custom TDT program.

The DAT-Cre mice were group-housed before surgery. The lowest-weight mouse from each cage was not used. Three weeks after surgery, we subjected the mice to daily RI tests with BC male intruders until the mice attacked for nine consecutive days. Four out of nine mice attacked on the first day of the RI test. Five out of nine mice showed aggressive behaviours within three days. For mice that took multiple non-aggressive interaction days to start to attack, the last non-aggressive day was used for analysis. The GRAB_{DA3h} response to VTA^{DAT} soma stimulation was measured on the day before any RI test under the naive condition, and one hour after the RI tests on the first and ninth aggression days. During the VTA^{DAT} stimulation, the mice were head-fixed on a running wheel⁵⁷, and 4-mW 589-nm laser stimulation (30 Hz, 10 ms) was delivered to the VTA through the implanted optic fibre. This stimulation lasted for 5 s and was repeated every 60 s for a minimum of six cycles. Mice expressing GRAB_{DA3h} in the NAcc were not tested for aggression. For non-aggressive social interaction tests, mice were not tested for aggression but interacted with an adult group-housed BC male mouse under a wired cup for 10 min per day for nine days.

To analyse the recording data, the MATLAB function 'msbackadj' with a moving window of 10% of the total recording duration was first applied to the raw signal (F_{raw}) to obtain the instantaneous baseline signal (F_{baseline}) for both 405-nm and 470-nm channels. The instantaneous $\Delta F/F$ was calculated as $(F_{\text{raw}} - F_{\text{baseline}})/F_{\text{baseline}}$. PETHs were constructed by aligning the $\Delta F/F$ to the onset of each behavioural trial, followed by averaging across all trials for each mouse and then across mice. For each recording session, the responses during the behaviour were calculated as the average $\Delta F/F$ for all trials of a specific behaviour. To establish the baseline, we calculated the mean of $\Delta F/F$ 2 min before introducing male intruders. For analysing the entry response, we calculated the $\Delta F/F$ during the first 60 s after intruder introduction. For investigation and attack response analysis, we excluded the behaviours that occurred within the first 60 s after intruder entry.

To determine parameters related to the light-evoked GRAB_{DA3h} response, we first constructed PETHs aligned to the 5-s light onset for each mouse. For response onset, the second derivative of the PSTH of each mouse was calculated, and the time index corresponding to the maximum value of the second derivative immediately after the light onset was identified as the response onset. For the latency to reach half-peak, the maximum value of the PSTH trace after time 0 was used as the peak response, and the first time point at which the GRAB_{DA3h} signal exceeded half of this maximum value was considered the half-peak latency. The first time point at which the GRAB_{DA3h} signal fell below the half-maximum value after the offset of the light stimulation was considered the half-decay latency.

Behavioural analysis

Mouse behaviours were recorded from both the top and the side using two synchronized cameras (Basler, acA640-120um) and commercial video acquisition software (Norpix, StreamPix 8) in a semi-dark room with infrared illumination at a frame rate of 25 frames per second. Mouse behaviours were automatically annotated using SimBA⁵⁸ and then refined by an experienced annotator who might or might not be blind to the group identity. 'Baseline' is defined as the 120 s right before introducing the male intruder into the home cage of the test mice. 'Intruder entry' was defined as the first 60 s after a freely moving

or cupped male mouse was introduced into the home cage of the test mouse. 'Investigate' was defined as close contact with any part of the intruder's body. 'Attack' was defined as a suite of intense actions aiming at biting the intruders, including push, lunge, bite, tumbling and fast locomotion episodes between these movements. 'Mount' was defined as when the male grasped and mounted the female's flanks. 'Intromit' includes both rapid thrust against the female's rear and deep rhythmic thrust.

In vitro electrophysiological recording

For in vitro whole-cell patch-clamp recordings, mice were anaesthetized with isoflurane and perfused with 15 ml ice-cold cutting solution containing 110 mM choline chloride, 25 mM NaHCO₃, 2.5 mM KCl, 7 mM MgCl₂, 0.5 mM CaCl₂, 1.25 mM NaH₂PO₄, 25 mM glucose, 11.6 mM ascorbic acid and 3.1 mM pyruvic acid. Then, the brains were removed and submerged in ice-cold cutting solution. Coronal sections (275 μ m) were cut using the Leica VT1200s vibratome and incubated in artificial cerebral spinal fluid (ACSF) containing 125 mM NaCl, 2.5 mM KCl, 1.25 mM NaH₂PO₄, 25 mM NaHCO₃, 1 mM MgCl₂, 2 mM CaCl₂ and 11 mM glucoses at 34 °C for 30 min and then at room temperature until use.

The intracellular solution for current-clamp recording contained 126 mM K-gluconate, 4 mM KCl, 10 mM HEPES, 4 mM Mg-ATP, 0.3 mM Na₂-GTP and 10 mM phosphocreatine (pH adjusted to 7.2 with KOH). The intracellular solution for the voltage-clamp recording contained 135 mM CsMeSO₃, 10 mM HEPES, 1 mM EGTA, 3.3 mM QX-314 (chloride salt), 4 mM Mg-ATP, 0.3 mM Na-GTP and 8 mM sodium phosphocreatine (pH 7.3 adjusted with CsOH). The signals were acquired using the MultiClamp 700B amplifier (Molecular Devices) and Clampex 11.0 software (Axon Instruments), and digitized at 20 kHz using DigiData1550B (Molecular Devices). The recorded electrophysiological data were analysed using Clampfit (Molecular Devices) and MATLAB (MathWorks).

VTA^{DAT} terminal stimulation and drug perfusion only started after the cell reached a stable state, typically 3 min after breaking into the cell.

To determine the effect of dopamine on dLS cell membrane potential, we performed current-clamp recordings. For the VTA^{DAT} terminal activation, we patched on randomly selected dLS neurons and delivered 200-ms, 589 nm light pulses (CoolLED, pE-300 white) five times with 20-s inter-pulse intervals. If a cell showed light-evoked slow IPSP, we bath-applied sulpiride (10 μ M, Tocris, 0895) for a minimum of 5 min and then repeated the light stimulation. To determine whether slow IPSP occurred, we calculated the mean and standard deviation (s.d.) of the membrane potential -1 to 0 s before the light onset and the average membrane potential 1-2 s after light onset. If the post-light mean membrane potential was two standard deviations below the baseline, the cell was considered to be hyperpolarized by the light stimulation. The slow VTA dopamine terminal stimulation evoked IPSP amplitude was calculated as the difference between the average membrane potential 1-2 s after light and -1-0 s before light. For bath applications of dopamine (100 μ M, Tocris, 3548), sulpiride (10 μ M, Tocris, 0895) + dopamine (100 μ M), sumanirole (1 μ M, Tocris, 2773) or sulpiride (10 μ M), we patched randomly selected dLS cells, recorded for 3 min to establish a baseline and then perfused the drug for at least 5 min. We then calculated the change in membrane potential amplitude as the difference between the mean membrane potential 2-3 min after drug perfusion and that -2-0 min before the drug perfusion. If the change in membrane potential amplitude was below $-2 \times$ s.d. of the membrane potential during the pre-drug period, the cell was considered hyperpolarized.

To examine the effect of VTA^{DAT} terminal stimulation on sIPSCs and sEPSCs, we performed voltage-clamp recording. The dLS cells were held at +0 mV (sIPSCs) or -70 mV (sEPSCs) for 65 s to establish a baseline. We then delivered 30-Hz, 1-ms, 589-nm light for 5 min at 30 Hz to activate VTA^{DAT} terminals and recorded for 5 min afterwards.

To examine the effect of the D2 agonist on sIPSCs, we patched onto D2R-expressing neurons in the dLS on the basis of their EYFP expression, held the cells at +0 mV and recorded for 65 s. We then added 1 μ M

Article

sumanirole into the bath solution, waited for 10 min and recorded for 2 min. To record mIPSCs, we added TTX (1 μ M, Tocris, 1078) into the bath solution.

To record sEPSCs, we patched on D2R-expressing neurons in the dLS on the basis of their EYFP expression, held the cells at -70 mV and recorded for 65 s. To record mEPSCs, we added TTX (1 μ M, Tocris, 1078) into the bath solution.

To investigate the intra-dLS connection, we patched onto ChR2-EYFP negative cells, held the cells at $+0$ mV, delivered brief blue light pulses (0.3 ms, five times, 20-s intervals), and recorded light-evoked IPSCs. We then applied 1 μ M sumanirole for 10 min, and recorded the light-evoked IPSCs of the same cell again.

To investigate the dLS^{Drd2} cell response to the CA2/3 inputs, we performed current-clamp recording of Drd2-positive cells on the basis of their mCherry expression. During the recording, we delivered a single light pulse or a train of five light pulses (1 mW, 0.3 ms, 470 nm) at frequencies of 1, 5 and 10 Hz, each three times with a 20-s inter-train interval. We then applied 1 μ M sumanirole or vehicle ACSF for 10 min and recorded the light-evoked spiking activities again using the same stimulation protocols. The post-spiking IPSP amplitude was calculated as the average membrane potential 0.2–0.7 s after light stimulation minus the average potential $-1-0$ s before light onset. The spiking probability was calculated as the number of light-evoked spikes divided by the number of light pulses.

To examine the effect of VTA^{DAT} terminal activation on dLS cell responses to excitatory inputs from CA2/3, we performed current-clamp recording of randomly selected dLS cells in the vicinity of VTA^{DAT} fluorescent terminals before and after sham or 589 nm light stimulation of VTA^{DA} terminals (5 min, 30 Hz, 1 ms).

Immunohistochemistry and imaging analysis

For histological analysis, mice were deeply anaesthetized and perfused with PBS followed by 4% PFA. After perfusion, brains were collected, post-fixed in 4% PFA overnight at 4 °C and then cryoprotected in 20% (w/v) sucrose for 24 h. The brains were then embedded in OCT compound and sectioned into 60- μ m-thick slices using a CM1900 cryostat (Leica). EYFP, EGFP and GRAB_{D3h} were immunostained using a chicken anti-GFP antibody (1:1,000, Abcam, ab13970) followed by an Alexa 488-conjugated donkey anti-chicken secondary antibody (1:1,000, Jackson ImmunoResearch, 703-545-155). mCherry and oScarlet were stained using a rabbit anti-dsRed antibody (1:1,000, Takara, 632496) followed by a Cy3-conjugated donkey anti-rabbit secondary antibody (1:1,000, Jackson ImmunoResearch, 711-165-152). TH cell body was stained with a sheep anti-TH primary antibody (1:750, Pel Freeze, P60101-0), followed by applying an Alexa 488-conjugated donkey anti-sheep secondary antibody (1:1,000, Jackson ImmunoResearch, 713-545-147). TH terminals were stained with a rabbit anti-TH primary antibody (1:500, EMD Millipore, AB152), followed by a Cy3-conjugated donkey anti-rabbit secondary antibody (1:1,000). FOS was immunostained using a guinea pig anti-FOS antibody (1:1,000, SYSY, 226308) followed by a Cy3-conjugated donkey anti-guinea pig secondary antibody (1:1,000, Jackson ImmunoResearch, 706-165-148). Brain slices were incubated in the primary antibody at 4 °C for 48 h, followed by a similar incubation period with the secondary antibody. In addition, DAPI (1:20,000, Thermo Fisher Scientific, D1306) was included with the secondary antibody for nuclear visualization. The fluorescence images were acquired with a virtual slide microscope (Olympus, VS120) with a 10 \times objective or a confocal microscope (Zeiss LSM 510 or 700 microscope).

To count the infected cells in the VTA and SNc, we outlined the VTA and SNc bilaterally on the basis of the DAPI staining, and exported the channel containing mCherry (chemogenetic group) or EGFP (TH mutagenesis group) using Fiji. The image contrast was kept the same across different samples. Cells were manually counted on the basis of cell morphology and relative brightness to the background by a researcher who was blinded to the treatment, using the Fiji cell counter.

For TH staining quantification, the brain sections containing NAcS (Bregma 0.98 mm) and dLS (Bregma 0.14 mm) from each mouse were selected for analysis. The channel containing the TH signal was extracted for each image. All images have a set intensity range of 50 to 3,000 before exporting to PNG format. The NAcS, dLS and corpus callosum in the same images were manually cropped to calculate the median TH fluorescence intensity.

For FOS quantification, the brain sections containing VTA (Bregma -3.16 mm) from each mouse were selected for analysis. VTA was outlined on the basis of TH and DAPI staining from the original images using Fiji. FOS counting results were obtained using the Cellpose 1.0 GUI⁵⁹, in which automatic segmentation was performed on the basis of the size of signal spots (5 pixels, flow threshold 0.7, cellprob threshold 0), followed by manual correction without any previous knowledge regarding the source of the images.

RNAscope in situ hybridization

Wild-type group-housed male mice were first single-housed for two weeks and then tested for aggression using RI tests with BC male intruders. For the novice aggressor group, the mice were perfused on the day after the first aggressive RI test. For the expert aggressor group, the mice were subjected to daily winning in RI tests for eight consecutive days and then perfused the day after the last RI test. Immediately after perfusion, their brains were collected and embedded in OCT compound on dry ice. The brains were then sectioned into 20- μ m-thick slices using a CM1900 cryostat (Leica) and mounted onto the slides (Fisher, 1255015). Slides containing dLS were fixated (15 min, 4% PFA) and dehydrated (50%, 70% and 100% ethanol, 5 min each). We did not treat the section with protease IV to ensure the integrity of the brain sections. We then used Mm-Drd2-C2 probe (ACD, 406501-C2) and RNAscope Fluorescent Multiplex Reagent Kit v1 (ACD, 320851) to detect *Drd2* mRNA following the standard protocol from the manufacturer (ACD). The sections were then imaged using a virtual slide microscope (Olympus, VS120) using a 20 \times objective. The *Drd2* signals were quantified using ImageJ.

Statistics and reproducibility

No statistical methods were used to predetermine sample sizes, but our sample sizes are similar to those reported in previous publications^{24,60–63}. All experiments were conducted using one to four cohorts of mice. For functional and in vivo recording experiments, histology images were collected from all mice. For slice recording experiments, histology images were collected only from a subset of mice, although the correct virus expression was always confirmed during the recording according to the fluorescence protein expression. Histology images are representative and qualitatively similar to images from other animals. The results were reproducible across cohorts and combined for final analysis. Statistical analyses were performed using MATLAB (v.2023a, MathWorks) and Prism10 (GraphPad Software). All statistical tests were two-tailed. Data were tested for normality first using the Shapiro–Wilk test. If all data points were normally distributed, paired *t*-tests, unpaired *t*-tests, ordinary one-way ANOVA with Tukey's post hoc test and repeated-measures one-way ANOVA with Turkey's or Dunnett's post hoc test were performed. If data points in one or more groups were not normally distributed, Mann–Whitney test, Wilcoxon matched-pairs signed-rank test, Kruskal–Wallis test with Dunn's multiple comparisons test and Friedman test with Dunn's multiple comparison post hoc test were performed. For comparing values across two categorical variables, we performed ordinary two-way ANOVA with Bonferroni's multiple comparison post hoc test for between-group comparisons and Turkey's multiple comparison post hoc test for within-group comparisons and repeated-measures two-way ANOVA with Turkey's or Bonferroni's multiple comparison test for matched data. In these cases, normality was not formally tested. To compare the effect of TH mutagenesis and VTA^{DAT} terminal lesion between test groups,

Fisher's exact test and Fisher's exact test followed by the two-stage linear step-up procedure of Benjamini, Krieger and Yekutieli FDR correction (FDR = 0.05) were performed. To compare the effectiveness of treatment on the percentage of mice that showed aggression, McNemar's test was applied when permitted. Details of each statistical test, including exact *P* values, *F* values, *t* values, degrees of freedom and cohort numbers, can be found in Supplementary Table 1. All error bars or error shades represent \pm s.e.m. All *P* values equal to or smaller than 0.05 are indicated in the figures.

Reporting summary

Further information on research design is available in the Nature Portfolio Reporting Summary linked to this article.

Data availability

Behavioural annotations, tracking, fibre photometry, slice electrophysiology and raw representative histology images can be downloaded from Zenodo (<https://doi.org/10.5281/zenodo.13937311>)⁶⁴. Behaviour videos and additional histology images are available from the corresponding authors upon reasonable request. They are not deposited to a public database owing to their large size and the size limitation of online repositories. Illustrations of the coronal brain sections are based on images from the Allen Brain Reference Atlas (<https://atlas.brain-map.org>). Source data are provided with this paper.

Code availability

MATLAB codes used in this study can be downloaded from Zenodo (<https://doi.org/10.5281/zenodo.13937311>)⁶⁴.

51. Paxinos, G. & Franklin, K. B. J. *The Mouse Brain in Stereotaxic Coordinates* (Elsevier Science, 2007).
52. Boyden, E. S., Zhang, F., Bamberg, E., Nagel, G. & Deisseroth, K. Millisecond-timescale, genetically targeted optical control of neural activity. *Nat. Neurosci.* **8**, 1263–1268 (2005).
53. Chen, X. et al. The first structure–activity relationship studies for designer receptors exclusively activated by designer drugs. *ACS Chem. Neurosci.* **6**, 476–484 (2015).

54. Mathis, A. et al. DeepLabCut: markerless pose estimation of user-defined body parts with deep learning. *Nat. Neurosci.* **21**, 1281–1289 (2018).
55. Cui, G. et al. Concurrent activation of striatal direct and indirect pathways during action initiation. *Nature* **494**, 238–242 (2013).
56. Gunaydin, L. A. et al. Natural neural projection dynamics underlying social behavior. *Cell* **157**, 1535–1551 (2014).
57. Osborne, J. E. & Dudman, J. T. RIVETS: a mechanical system for in vivo and in vitro electrophysiology and imaging. *PLoS One* **9**, e89007 (2014).
58. Goodwin, N. L. et al. Simple Behavioral Analysis (SimBA) as a platform for explainable machine learning in behavioral neuroscience. *Nat. Neurosci.* **27**, 1411–1424 (2024).
59. Stringer, C., Wang, T., Michaelos, M. & Pachitariu, M. Cellpose: a generalist algorithm for cellular segmentation. *Nat. Methods* **18**, 100–106 (2021).
60. Yin, L. et al. VMHvl^{Cckar} cells dynamically control female sexual behaviors over the reproductive cycle. *Neuron* **110**, 3000–3017 (2022).
61. Yamaguchi, T. et al. Posterior amygdala regulates sexual and aggressive behaviors in male mice. *Nat. Neurosci.* **23**, 1111–1124 (2020).
62. Falkner, A. L. et al. Hierarchical representations of aggression in a hypothalamic–midbrain circuit. *Neuron* **106**, 637–648 (2020).
63. Fang, Y. Y., Yamaguchi, T., Song, S. C., Tritsch, N. X. & Lin, D. A hypothalamic midbrain pathway essential for driving maternal behaviors. *Neuron* **98**, 192–207 (2018).
64. Dai, B. et al. Supporting data for 'Experience-dependent dopamine modulation of male aggression'. *Zenodo* <https://doi.org/10.5281/zenodo.13937311> (2024).

Acknowledgements We thank Y. Jiang for assisting with genotyping, T. Sippy for the insightful discussion regarding the dopamine role in humans, J. Basu and R. Yan for advice on in vitro recording experiments and W. Zhou for discussion and proofreading. Elements (mice) in Figs. 1e and 2f and Extended Data Fig. 7b,h were created with BioRender (<https://biorender.com>). This research was supported by NIH grants R01MH101377, R01MH124927 and U19NS107616 (D.L.), U01NS11335 (D.L. and Y.L.), U01NS12082 (Y.L.), P30-DA048736 (L.S.Z.) and R01MH133669 (N.X.T.), and by the Vulnerable Brain Project (D.L.).

Author contributions D.L. and B.D. conceived the project, designed experiments and wrote the manuscript. D.L. supervised the project. B.D. performed nearly all experiments and analysed the data. B.Z., X.D., X.C. and J.C. assisted with behavioural recording and/or analysis. L.Y. performed preliminary slice recording experiments. N.X.T. provided crucial feedback on the slice recording experiments and edited the paper. L.S.Z. provided CRISPR–SaCas9 viruses. Y.Z. and Y.L. developed GRAB_{DA3H}.

Competing interests The authors declare no competing interests.

Additional information

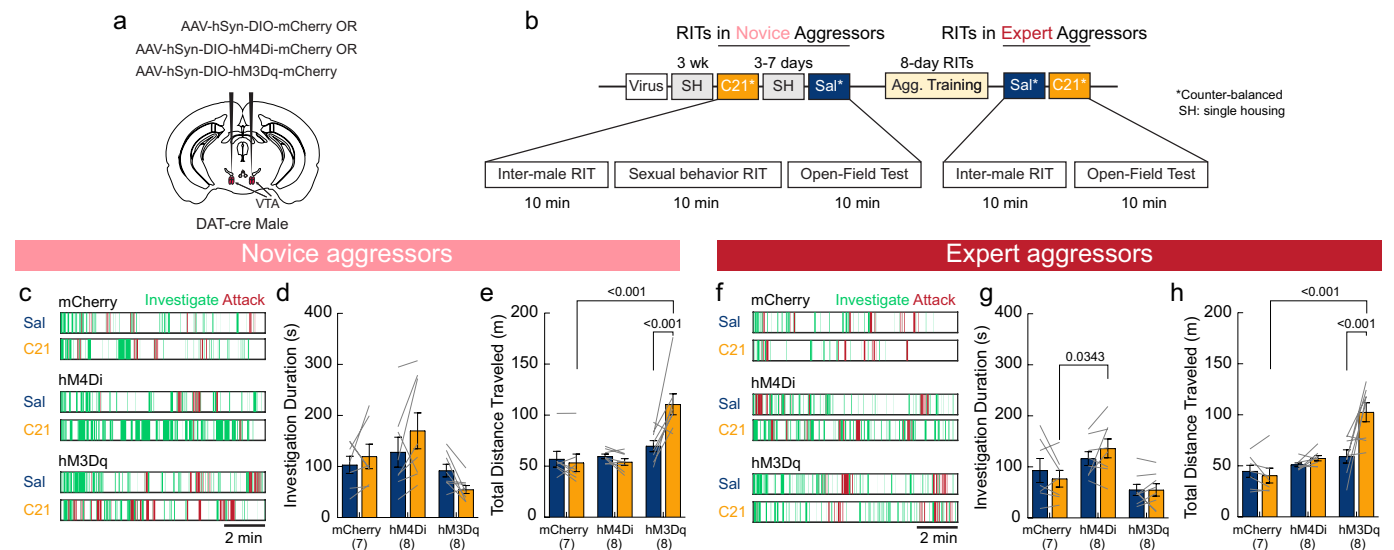
Supplementary information The online version contains supplementary material available at <https://doi.org/10.1038/s41586-024-08459-w>.

Correspondence and requests for materials should be addressed to Bing Dai or Dayu Lin.

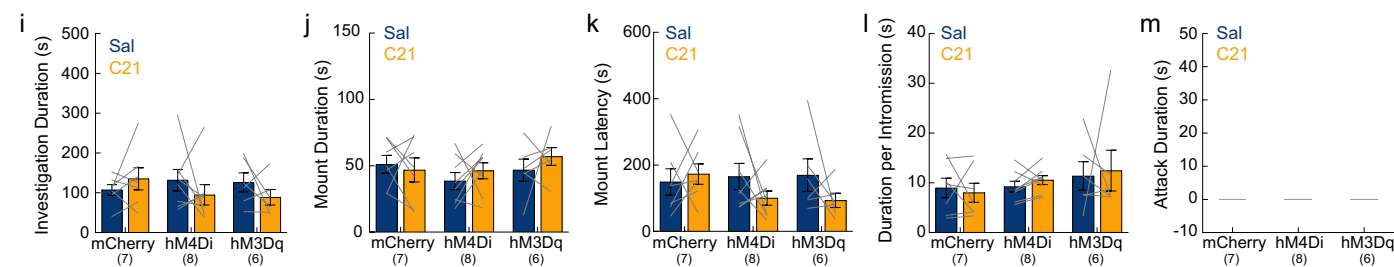
Peer review information *Nature* thanks Cornelius Gross, Felix Leroy and Stephen Shea for their contribution to the peer review of this work. Peer reviewer reports are available.

Reprints and permissions information is available at <http://www.nature.com/reprints>.

Chemogenetic manipulation of VTA^{DAT} cells during inter-male interaction and open-field test



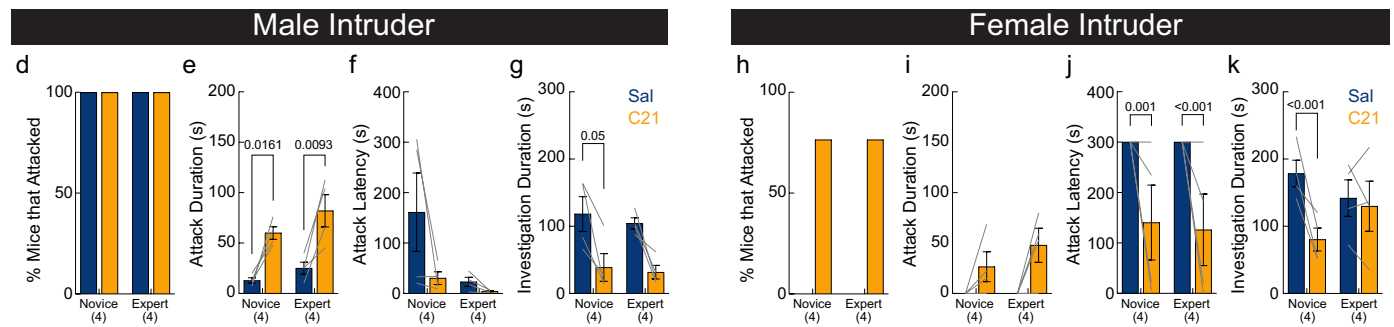
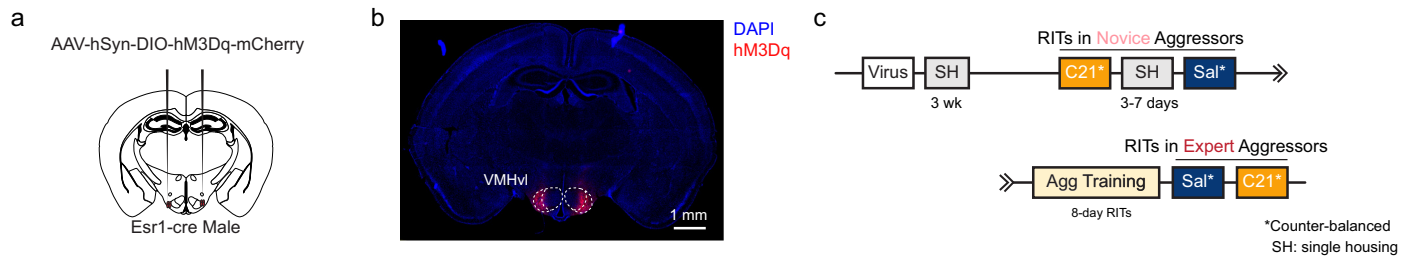
Chemogenetic manipulation of VTA^{DAT} cells does not affect male sexual behavior



Extended Data Fig. 1 | Effect of chemogenetic manipulation of VTA^{DAT} cells on inter-male investigation, male sexual behaviours and locomotion.

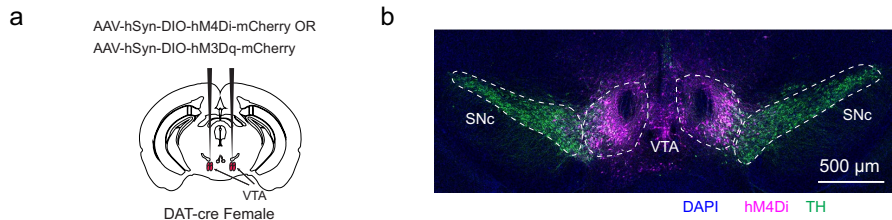
a,b, Experimental design (**a**) and timeline (**b**) to chemogenetically manipulate VTA^{DAT} cells. **c**, Representative raster plots showing investigation and attack after saline or C21 treatment in mCherry, hM4Di, and hM3Dq novice aggressors. **d,e**, Investigation duration during the resident-intruder test (**d**), and the total distance travelled in the open-field arena (**e**) after saline or C21 treatment in mCherry, hM4Di, and hM3Dq novice aggressors. **f**, Representative raster plots showing investigation and attack after saline or C21 treatment in mCherry, hM4Di, and hM3Dq expert aggressors. **g,h**, Investigation duration during the resident-intruder test (**g**), and the total distance travelled in the open-field

arena (**h**) after saline or C21 treatment in mCherry, hM4Di, and hM3Dq expert aggressors. **i-m**, Investigation duration (**i**), mount duration (**j**), latency to mount (**k**), averaged duration per intromission (**l**) and attack duration (**m**) towards female intruders after saline or C21 i.p. injections in novice aggressors. Each line represents one mouse. Bars and error bars in **d,e,g,h,i-l** represent mean \pm SEM. Numbers inside the parentheses indicate the number of subject mice. **d,e,g,h,i-m**, repeated-measures (RM) two-way ANOVA followed by multiple comparison tests with Bonferroni's correction. All tests are two-sided. All p values ≤ 0.05 are indicated. See Supplementary Table 1 for statistical details. Brain illustration in **a** is adapted from the Allen Brain Reference Atlas (<https://atlas.brain-map.org>).

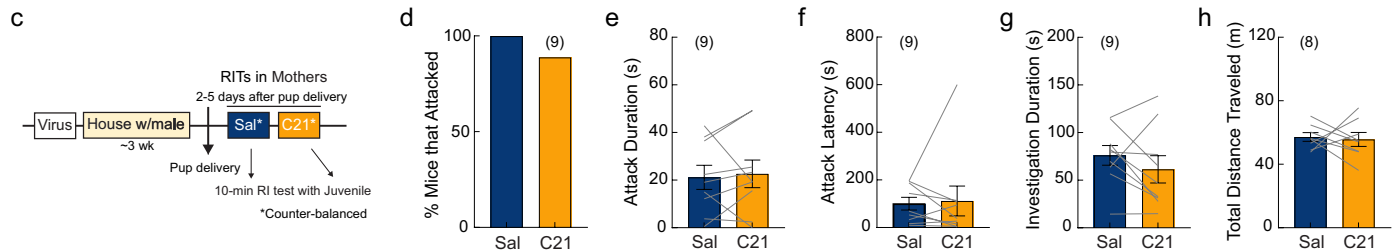


Extended Data Fig. 2 | Chemogenetic activation of VMHvl^{Esr1} cells promotes aggression in both novice and expert aggressors. **a**, Experimental design to chemogenetically activate VMHvl^{Esr1} cells in male mice. **b**, Representative histology image showing hM3Dq expression (red) in the VMHvl^{Esr1} cells. **c**, The experimental timeline. **d–g**, The percentage of mice that attacked (**d**), attack duration (**e**), latency to attack (**f**) and investigation duration (**g**) of male intruders after saline or C21 i.p. injections in novice and expert aggressors. **h–k**, The percentage of mice that attacked (**h**), attack duration (**i**), latency to attack (**j**)

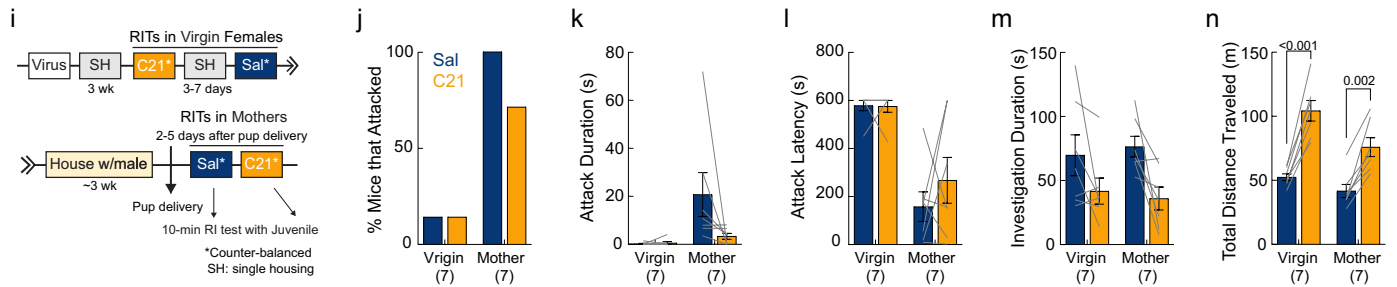
and investigation duration (**k**) of female intruders after saline or C21 i.p. injections in novice and expert aggressors. Each line represents one mouse. Bars and error bars represent mean \pm SEM. Numbers inside the parentheses indicate the number of subject mice. **h**, McNemar's test; **e–g**, **i–k**, RM two-way ANOVA followed by multiple comparison tests with Bonferroni's correction. All tests are two-sided. All p values \leq 0.05 are indicated. See Supplementary Table 1 for statistical details. Brain illustration in **a** is adapted from the Allen Brain Reference Atlas (<https://atlas.brain-map.org>).



Chemogenetic inhibition of VTA^{DAT} cells in mothers

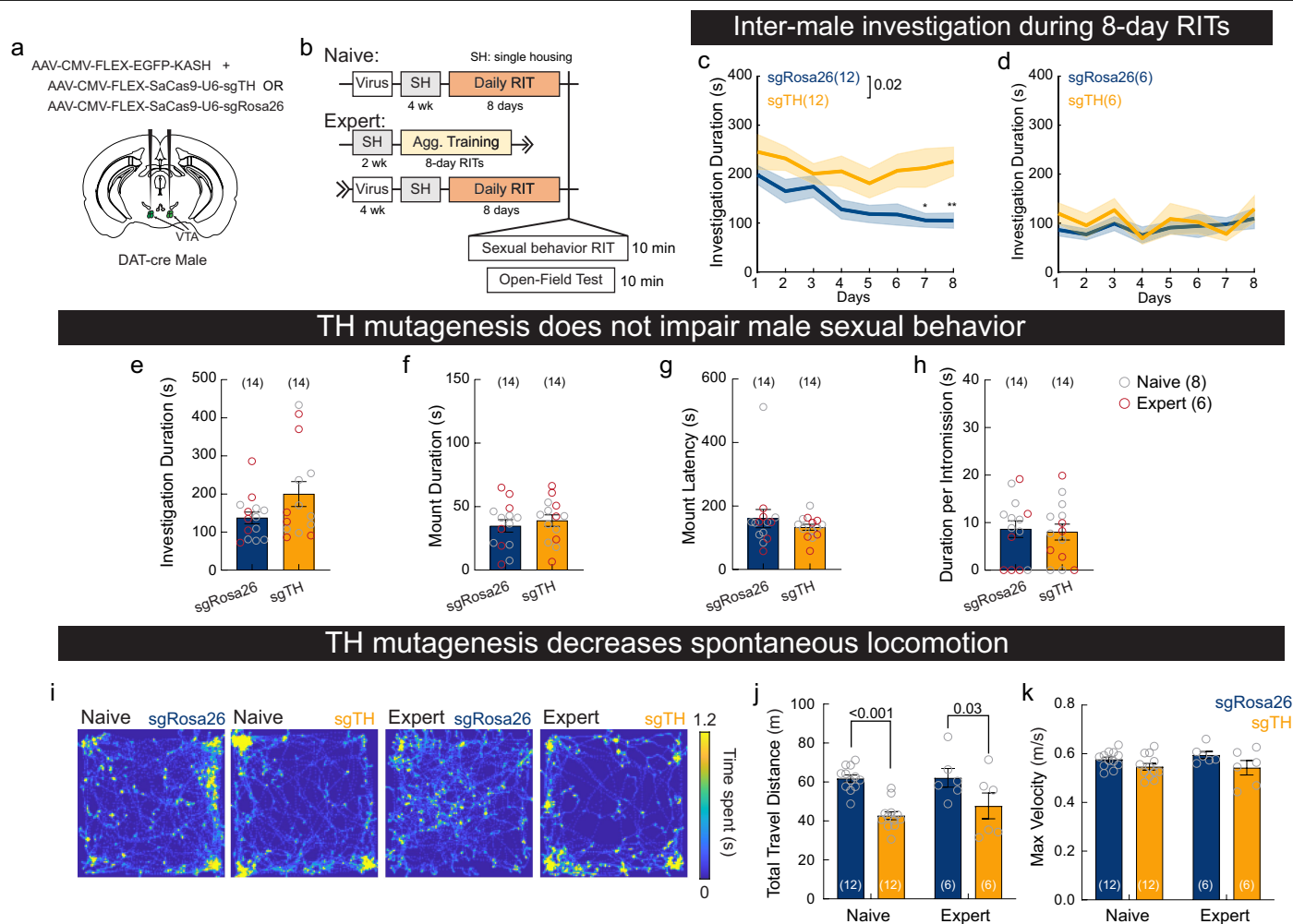


Chemogenetic activation of VTA^{DAT} cells in virgin females and mothers



Extended Data Fig. 3 | Chemogenetic manipulation of VTA^{DAT} cells does not change female aggression. **a**, Experimental design. **b**, A representative histology image showing the expression of TH and hM4Di. **c**, Experimental timeline to chemogenetically inhibit VTA^{DAT} cells in mothers. **d-h**, The percentage of mice that attacked (**d**), attack duration (**e**), latency to attack (**f**), investigation duration (**g**) of a juvenile intruder and the total distance travelled in a large open arena (**h**) after saline or C21 treatment in aggressive lactating female mice (mothers). **i**, Experimental timeline to chemogenetically activate VTA^{DAT} cells in virgin and lactating females. **j-n**, The percentage of mice that attacked (**j**), attack duration (**k**), latency to attack (**l**), investigation duration (**m**) of a

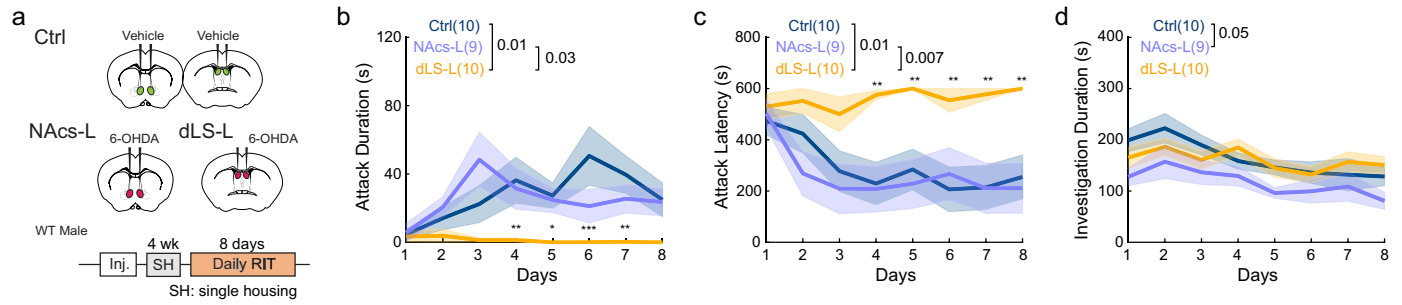
juvenile intruder and the total distance travelled in a large open arena (**n**) after saline or C21 treatment in virgin and aggressive lactating female mice (mothers). Each line represents one mouse. Bars and error bars represent mean ± SEM. Numbers inside the parentheses indicate the number of subject mice. **d, j**, McNemar's test; **f**, paired Wilcoxon test; **e, g, h**, paired t-test; **k-n**, RM two-way ANOVA followed by multiple comparison tests with Bonferroni's correction. All tests are two-sided. All p values ≤ 0.05 are indicated. See Supplementary Table 1 for statistical details. Brain illustration in **a** is adapted from the Allen Brain Reference Atlas (<https://atlas.brain-map.org>).



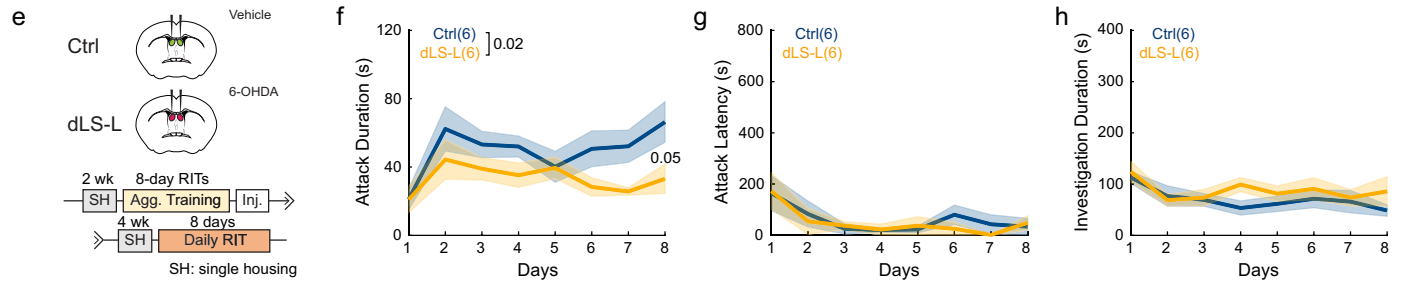
Extended Data Fig. 4 | Effect of TH mutagenesis in VTA^{DAT} cells on inter-male investigation, male sexual behaviours and locomotion. **a, b**, Experimental design (**a**) and timeline (**b**) to induce Rosa26 or TH mutagenesis in VTA^{DAT} cells. **c, d**, Investigation duration during each of the daily RI tests after ablating Rosa26 or TH in naïve male mice (**c**) and expert aggressors (**d**). **e–h**, Investigation duration (**e**), mount duration (**f**), latency to mount (**g**) and average duration per intromission (**h**) towards receptive female mice after Rosa26 or TH mutagenesis in naïve male mice (grey circle) and expert aggressors (red circle). **i**, Heat maps illustrating the body centre distribution of example sgRosa26- and sgTh-expressing mice during the 10-min locomotion test in a large open arena. **j, k**, The total travel distance (**j**) and the maximum velocity (**k**) in the open arena

of the naïve mice and expert aggressors with Rosa26 or sgTH mutagenesis. Each circle represents one mouse. Bars and error bars in **e–h, j–k** and solid lines and shades in **c, d** represent mean \pm SEM. Numbers inside the parentheses indicate the number of subject mice. **c, d**, RM two-way ANOVA followed by multiple comparison tests with Bonferroni's correction; **e, g**, Mann–Whitney test; **f, h**, unpaired t-test; **j, k**, ordinary two-way ANOVA followed by multiple comparison tests with Bonferroni's correction. All tests are two-sided. All p values ≤ 0.05 are indicated. See Supplementary Table 1 for statistical details. Brain illustration in **a** is adapted from the Allen Brain Reference Atlas (<https://atlas.brain-map.org>).

dLS dopamine lesion blocks aggression increase in naive males

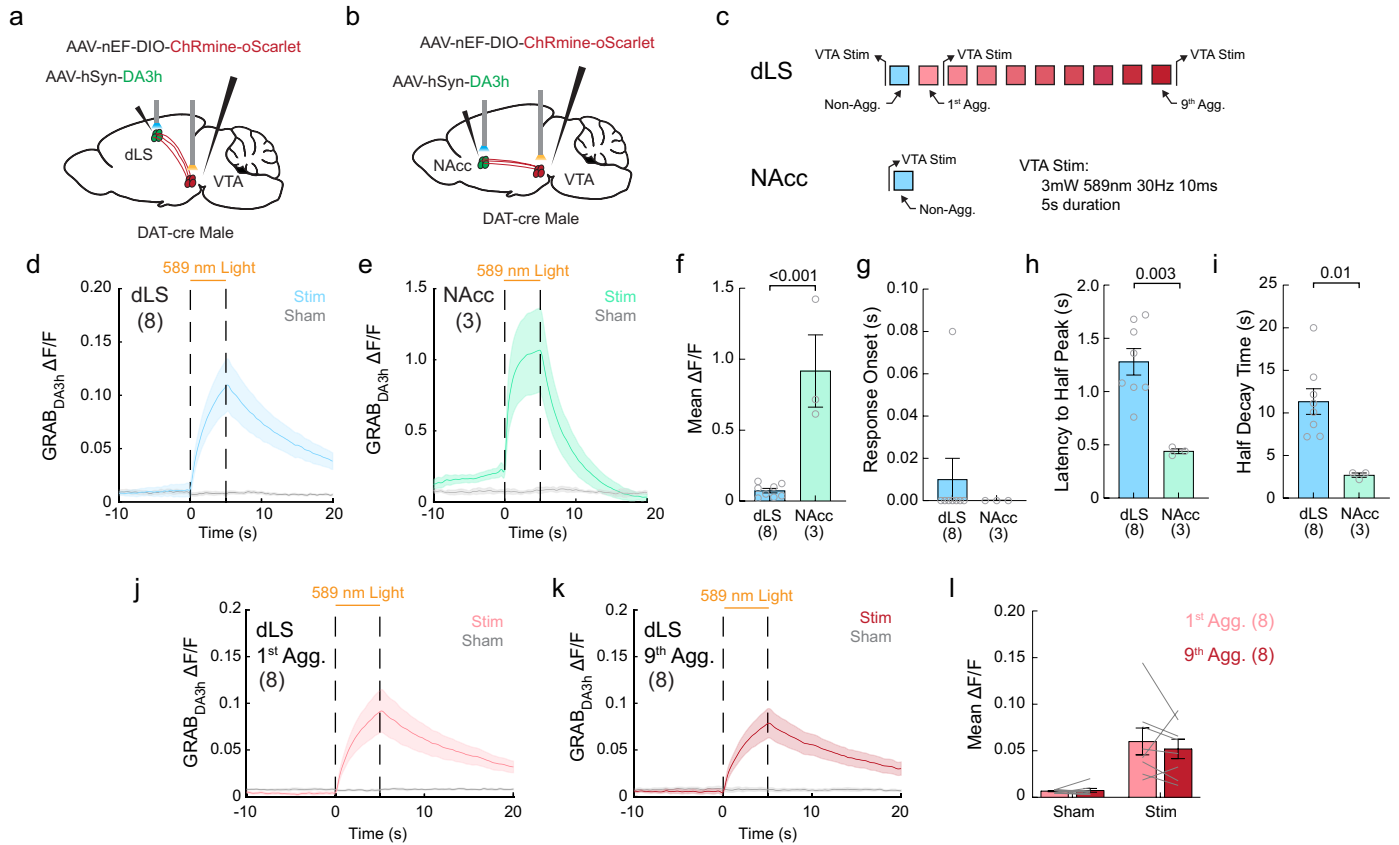


dLS dopamine lesion does not change aggression in expert aggressors



Extended Data Fig. 5 | dLS 6-OHDA lesion prevents the rise of aggression in naive mice but has no effect on expert aggressors. a, Experimental design and timeline to lesion dopamine terminals at dLS and NAc in naive wild-type male mice. **b–d**, Attack duration (**b**), latency to attack (**c**) and investigation duration (**d**) of BC male intruders during the 8-day RI tests after injecting vehicle or 6-OHDA into the NAc or dLS of naive mice. RM two-way ANOVA followed by multiple comparison tests with Tukey’s correction. * $p < 0.05$, ** $p < 0.01$, and *** $p < 0.001$. Statistics are for dLS-L vs. Ctrl comparisons. **e**, Experimental design and timeline to deplete dopamine terminals at the dLS in expert aggressors.

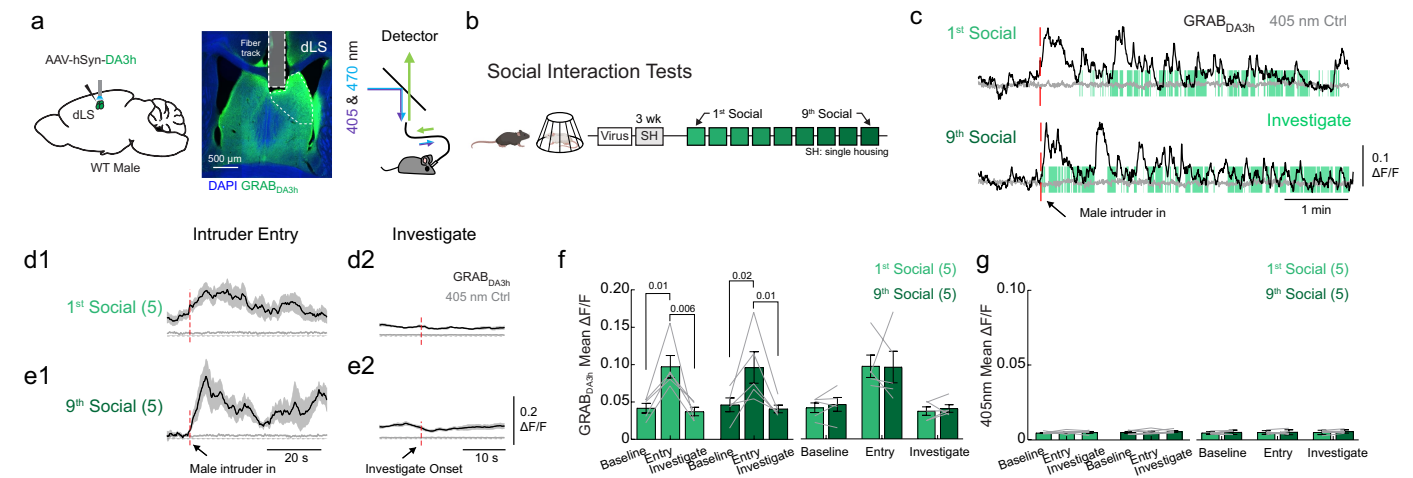
f–h, Attack duration (**f**), latency to attack (**g**) and investigation duration (**h**) of BC male intruders during the 8-day RI tests after injecting vehicle or 6-OHDA into the dLS of expert aggressors. RM two-way ANOVA followed by multiple comparison tests with Bonferroni’s correction. Colour lines and shades represent mean \pm SEM. Numbers inside the parentheses indicate the number of subject mice. All tests are two-sided. All p values ≤ 0.05 are indicated. See Supplementary Table 1 for statistical details. Brain illustrations in **a, e** are adapted from the Allen Brain Reference Atlas (<https://atlas.brain-map.org>).



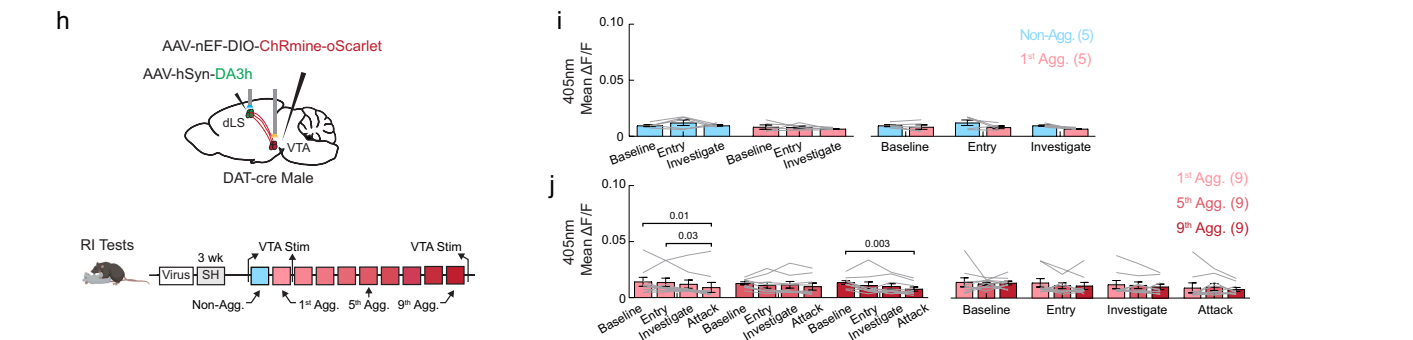
Extended Data Fig. 6 | VTA^{DAT} stimulation induces different patterns of dopamine release at the dLS and at the NAcc. **a–c**, Experimental designs (**a,b**), and timeline (**c**) to stimulate the VTA^{DAT} cells and record the dopamine signal at the dLS or NAcc. **d,e**, PETHs of GRAB_{DA3h} signals ($\Delta F/F$) at the dLS (**d**) and NAcc (**e**) aligned to the VTA^{DAT} light (colour) or sham light (0 mW, grey) onset. **f**, The mean GRAB_{DA3h} signal during the 5 s VTA^{DAT} stimulation. **g**, The onset of the GRAB_{DA3h} response following VTA^{DAT} stimulation. **h**, The latency to reach half of the GRAB_{DA3h} peak response amplitude following VTA^{DAT} stimulation. **i**, The half-decay time of GRAB_{DA3h} signal after VTA^{DAT} stimulation offset. **j,k**, PETHs of GRAB_{DA3h} signal of the dLS aligned to the VTA^{DAT} light (colour)

or sham light (0 mW, grey) onset on the 1st (**j**) and 9th days of aggression (**k**). **l**, The mean GRAB_{DA3h} activity of the dLS on the 1st and 9th days of aggression during 5 s VTA^{DAT} stimulation or sham periods. Each circle and line represents one mouse. Lines and shades in **d,e** and **j,k** and bars and error bars in **f–i** and **l** represent mean \pm SEM. Numbers inside the parentheses indicate the number of subject mice. **f,h**, unpaired t-test; **g,i**, Mann–Whitney test; **l**, RM two-way ANOVA followed by multiple comparison tests with Bonferroni's correction. All tests are two-sided. All p values ≤ 0.05 are indicated. See Supplementary Table 1 for statistical details.

dLS GRAB_{DA3h} response during social interaction tests

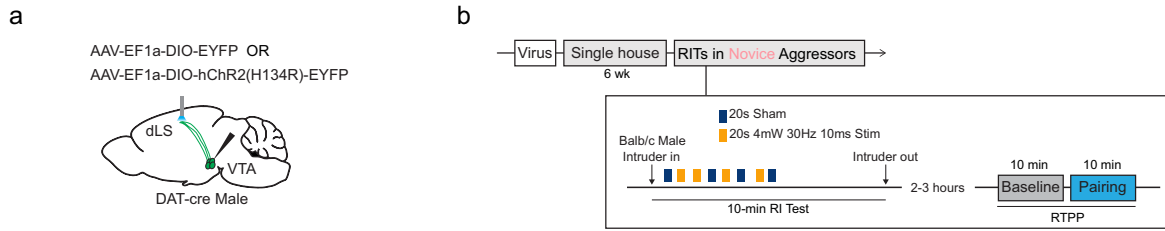


405 nm control signals for GRAB_{DA3h} recording



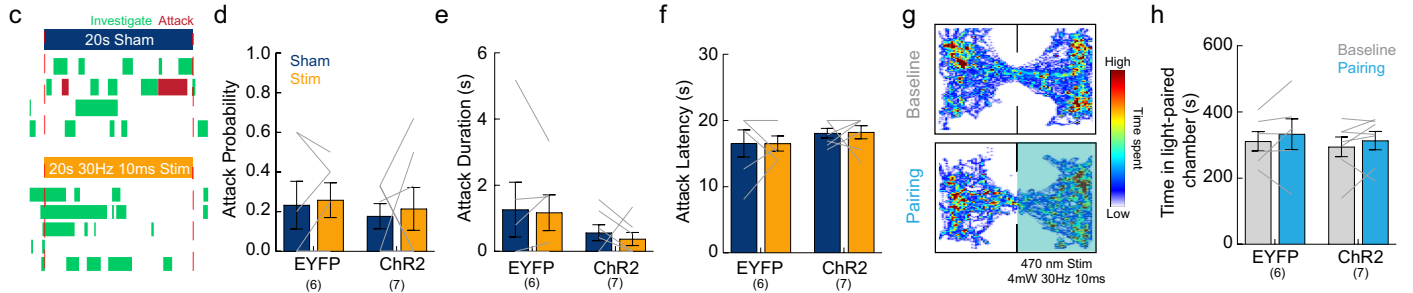
Extended Data Fig. 7 | dLS GRAB_{DA3h} signals do not change with repeated social interactions. **a**, Experimental design and fibre photometry set-up to record dopamine release at the dLS and a representative histology image. The white dashed lines indicate the fibre track. **b**, The experimental timeline to record dopamine release at the dLS during social interaction tests. **c**, Representative ΔF/F traces of GRAB_{DA3h} (black) and 405 nm control (grey) signals of dLS cells during the social interaction tests on the 1st (top) and 9th (bottom) days of testing. Red dashed lines indicate the introduction of the caged male intruders. **d,e**, Average PETHs of GRAB_{DA3h} (black) and 405 nm channel (grey) signals (ΔF/F) aligned to the onset of intruder entry (**d1** and **e1**) and investigation (**d2** and **e2**). Red dash lines indicate the time 0 of the behaviour. **f,g**, The averaged ΔF/F of GRAB_{DA3h} signals (**f**) and 405 nm channel (**g**) during

various behaviours on the 1st and 9th days of social interaction. **h**, Experimental design and timeline to record dopamine release at the dLS. **i**, The averaged ΔF/F of 405 nm channel during various behaviours of the RI tests on the last non-aggressive day and the 1st day of attack. **j**, The averaged ΔF/F of 405 nm channel during various behaviours of the RI tests on the 1st, 5th, and 9th days of aggression. Each line represents one mouse. Bars and error bars represent mean ± SEM. Numbers inside the parentheses indicate the number of subject mice. **f,g,i,j**, RM two-way ANOVA followed by multiple comparison tests with Bonferroni's or Tukey's correction. All tests are two-sided. All p values ≤ 0.05 are indicated. See Supplementary Table 1 for statistical details. Elements (mice) in **b,h** were created using BioRender (<https://biorender.com>).

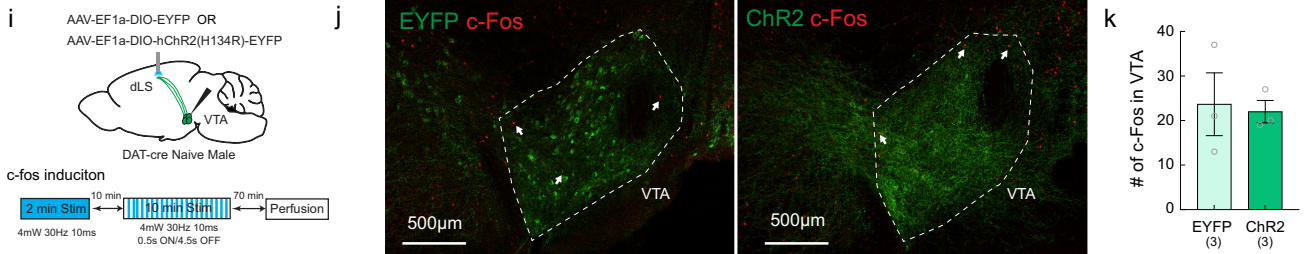


Acute activation of the VTA^{DAT} terminals at dLS

RTTP



Tonic activation of VTA^{DAT} terminals at dLS did not induce c-Fos in the VTA

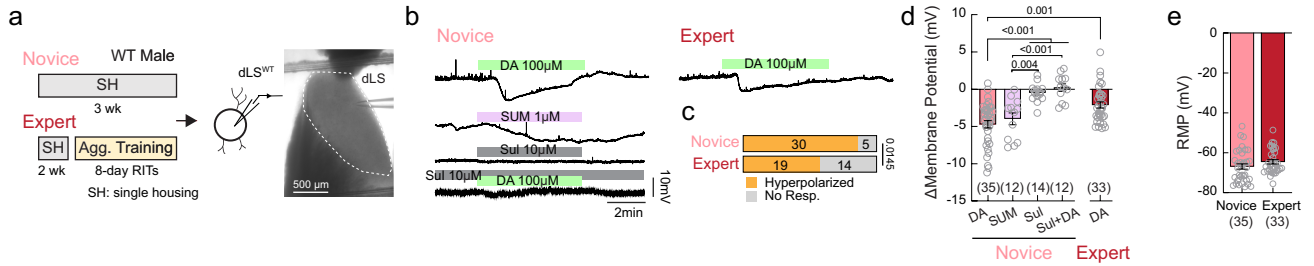


Extended Data Fig. 8 | See next page for caption.

Article

Extended Data Fig. 8 | Acute stimulation of VTA^{DAT}-dLS terminals or tonic activation of VTA^{DAT}-NAcs terminals does not change aggressive behaviours in novice aggressors. **a,b**, Experimental design (**a**) and timeline (**b**) to determine the acute effect of VTA^{DAT}-dLS terminal stimulation on aggression. **c**, Behavioural raster of a representative mouse during the 20 s sham (0 mW) and light (4 mW) trials. **d-f**, The attack probability (**d**), attack duration (**e**) and latency to attack (**f**) during the 20 s light or sham stimulation periods. **g**, Heat maps illustrating the body centre distribution of an example mouse during the baseline and light-pairing periods when VTA^{DAT}-dLS terminals are activated in one pre-selected chamber. **h**, Time spent in the light-paired chamber during the 10-min baseline and 10-min light-pairing periods. **i**, Experimental design and timeline to quantify FOS expression after tonic stimulation of VTA^{DAT} terminals at the dLS. **j**, Representative images showing FOS (red) and EYFP (left, green), or Chr2 (right, green), expression in the VTA. White arrows highlight example FOS positive cells. **k**, The number of FOS positive cells in the VTA of EYFP and Chr2-expressing mice. **l**, Experimental schematics and representative histology

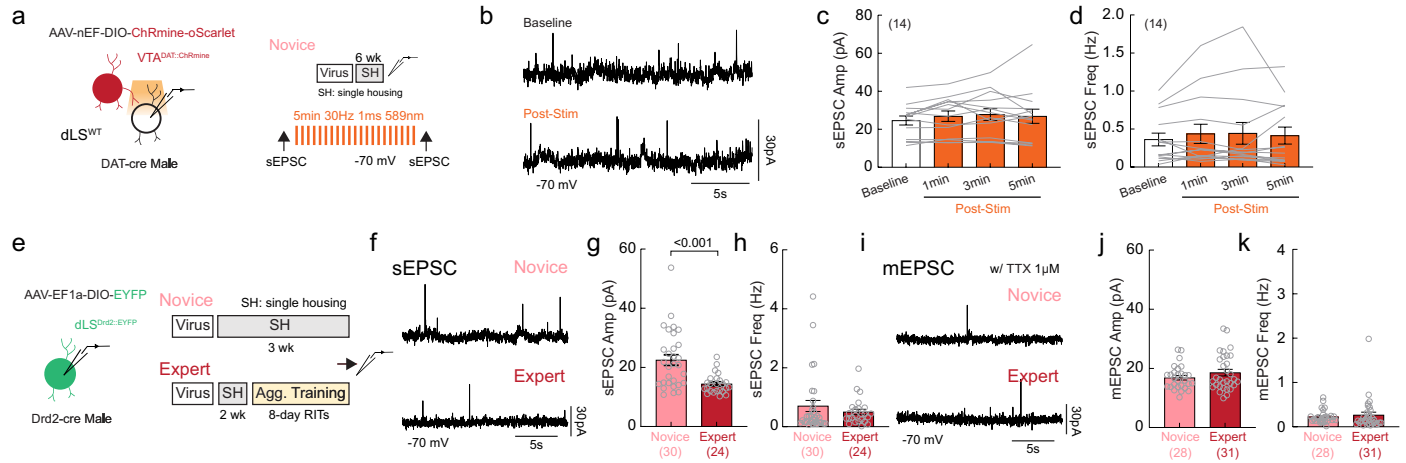
images showing Chr2 cells in the VTA and their terminals in the NAc. The white arrows indicate the fibre tracks. **m**, Experimental timeline to evaluate the effect of tonic activation of VTA^{DAT}-NAcs terminals on aggression. **n-q**, The percentage of mice that attacked (**n**), attack duration (**o**), latency to attack (**p**) and investigation duration (**q**) of novice aggressors on sham and light-stimulated days. **r**, Heat maps illustrating the body centre distribution of an example mouse during the baseline and light-pairing period when VTA^{DAT}-NAcs terminals are activated in one pre-selected chamber. **s**, Time spent in the light-paired chamber during 10 min baseline and 10 min light-pairing periods. Each line represents one mouse. Bars and error bars represent mean \pm SEM. Numbers inside the parentheses indicate the number of subject mice. **d-f,h**, RM two-way ANOVA followed by multiple comparison tests with Bonferroni's correction; **k**, unpaired t-test; **n**, McNemar's test; **o,q,s**, paired t-test; **p**, Wilcoxon matched-pairs signed-rank test. All tests are two-sided. All p values \leq 0.05 are indicated. See Supplementary Table 1 for statistical details.



Extended Data Fig. 9 | Aggression experience diminishes the dopamine-induced hyperpolarization of dLS cells. **a**, Experimental timeline and schematics showing current-clamp recording of dLS cells in response to dopamine application and a representative image of the recorded lateral septum slice and a recording glass pipette. **b**, Left: Representative current-clamp recording traces of dLS^{WT} cells of novice aggressors after bath application of dopamine, sumanirole (SUM), sulpiride (Sul), and sulpiride+dopamine. Right: A representative trace of a dLS^{WT} cell of an expert aggressor after applying dopamine. **c**, Distribution of dLS^{WT} cell responses to dopamine in novice and expert aggressors. **d**, The membrane potential change of dLS^{WT}

cells (difference between 2–3 min and -2–0 min of drug perfusion) after bath application of various drugs in novice and expert aggressors. **e**, The resting membrane potential (RMP) of dLS^{WT} cells in novice and expert aggressors. Each dot represents one cell. Bars and error bars represent mean \pm SEM. Numbers inside the parentheses or bars indicate the number of recorded cells. **c**, Fisher's exact test; **d**, Ordinary one-way ANOVA followed by multiple comparison tests with Tukey's correction and Mann-Whitney test between novice and expert aggressors; **e**, Mann-Whitney test. All p values \leq 0.05 are indicated. See Supplementary Table 1 for statistical details.

Article



Extended Data Fig. 10 | Effects of VTA^{DAT} terminal activation and aggression experience on excitatory synaptic transmission of dLS cells. **a**, Schematics showing voltage-clamp recording of dLS^{WT} cell responses to VTA^{DAT} inputs and the light stimulation protocol. **b**, Representative sEPSC traces of a dLS cell before (top) and after (bottom) the 5-min light stimulation. **c,d**, The amplitude (**c**) and frequency (**d**) of sEPSCs before and after light stimulation. **e**, Schematics and experimental timeline showing voltage-clamp recording of dLS^{Drd2} cells. **f**, Representative sEPSC traces of example dLS^{Drd2} cells from novice (top) and expert (bottom) aggressors. **g,h**, The amplitude (**g**) and frequency (**h**) of sEPSCs

in novice and expert aggressors. **i**, Representative mEPSC traces of dLS^{Drd2} cells from novice (top) and expert (bottom) aggressors. **j,k**, The amplitude (**j**) and frequency (**k**) of mEPSCs in novice and expert aggressors. Each line or circle represents one cell. Bars and error bars represent mean \pm SEM. Numbers inside the parentheses indicate the number of recorded cells. **c,d**, Friedman test followed by multiple comparison tests with Dunn's correction. **g-h,j-k**, Mann-Whitney test. All tests are two-sided. All p values ≤ 0.05 are indicated. See Supplementary Table 1 for statistical details.

Reporting Summary

Nature Portfolio wishes to improve the reproducibility of the work that we publish. This form provides structure for consistency and transparency in reporting. For further information on Nature Portfolio policies, see our [Editorial Policies](#) and the [Editorial Policy Checklist](#).

Statistics

For all statistical analyses, confirm that the following items are present in the figure legend, table legend, main text, or Methods section.

n/a Confirmed

- The exact sample size (n) for each experimental group/condition, given as a discrete number and unit of measurement
- A statement on whether measurements were taken from distinct samples or whether the same sample was measured repeatedly
- The statistical test(s) used AND whether they are one- or two-sided
Only common tests should be described solely by name; describe more complex techniques in the Methods section.
- A description of all covariates tested
- A description of any assumptions or corrections, such as tests of normality and adjustment for multiple comparisons
- A full description of the statistical parameters including central tendency (e.g. means) or other basic estimates (e.g. regression coefficient) AND variation (e.g. standard deviation) or associated estimates of uncertainty (e.g. confidence intervals)
- For null hypothesis testing, the test statistic (e.g. F , t , r) with confidence intervals, effect sizes, degrees of freedom and P value noted
Give P values as exact values whenever suitable.
- For Bayesian analysis, information on the choice of priors and Markov chain Monte Carlo settings
- For hierarchical and complex designs, identification of the appropriate level for tests and full reporting of outcomes
- Estimates of effect sizes (e.g. Cohen's d , Pearson's r), indicating how they were calculated

Our web collection on [statistics for biologists](#) contains articles on many of the points above.

Software and code

Policy information about [availability of computer code](#)

Data collection

Animal behaviors were recorded from both the top and side using two synchronized cameras (Basler, acA640-120um) and commercial video acquisition software (Norpix, StreamPix 8). Fiber photometry recording data was recorded using RZ5 real-time processor (Tucker-Davis Technologies). The envelope of 400 Hz 470-nm LED-induced signals and 317 Hz 405-nm LED-induced signals from the photoreceiver were extracted in real time using a custom-written program (Tucker-Davis Technologies) as the readout of GRAB DA3h intensity. Optogenetic light stimulation was controlled using a custom-written program (Tucker-Davis Technologies). Electrophysiology data were recorded with MultiClamp 700B amplifier (Molecular Devices) and Clampex 11.0 software (Axon Instruments), digitized at 20 kHz with Digidata 1550B (Axon Instruments). Behavior and fiber photometry data were analyzed using custom code written in MATLAB 2023a (Mathworks). Statistical analyses were done using Prism 10 (GraphPad).

Data analysis

Animal behaviors were automatically annotated using SimBA (v1.3) and then refined by experienced annotators.

For manuscripts utilizing custom algorithms or software that are central to the research but not yet described in published literature, software must be made available to editors and reviewers. We strongly encourage code deposition in a community repository (e.g. GitHub). See the Nature Portfolio [guidelines for submitting code & software](#) for further information.

Data

Policy information about [availability of data](#)

All manuscripts must include a [data availability statement](#). This statement should provide the following information, where applicable:

- Accession codes, unique identifiers, or web links for publicly available datasets
- A description of any restrictions on data availability
- For clinical datasets or third party data, please ensure that the statement adheres to our [policy](#)

Raw values associated with each figure panel can be found in the source data files. Behavioral annotations, tracking, fiber photometry, slice electrophysiology, raw representative histology images can be downloaded from Zenodo (10.5281/zenodo.13937311). Behavior videos and additional histology images are available from the corresponding authors upon reasonable request. They are not deposited to a public database owing to their large size and size limitation of the online depositories. Illustrations of the coronal brain sections in Figs. 1a, l, and 2a and Extended Data Figs. 1a, 2a, 3a, 4a, and 5a,e were adapted from the Allen Brain Reference Atlas (<https://atlas.brain-map.org>). Source data are provided with this paper.

Research involving human participants, their data, or biological material

Policy information about studies with [human participants or human data](#). See also policy information about [sex, gender \(identity/presentation\), and sexual orientation](#) and [race, ethnicity and racism](#).

Reporting on sex and gender	N/A
Reporting on race, ethnicity, or other socially relevant groupings	N/A
Population characteristics	N/A
Recruitment	N/A
Ethics oversight	N/A

Note that full information on the approval of the study protocol must also be provided in the manuscript.

Field-specific reporting

Please select the one below that is the best fit for your research. If you are not sure, read the appropriate sections before making your selection.

- Life sciences Behavioural & social sciences Ecological, evolutionary & environmental sciences

For a reference copy of the document with all sections, see nature.com/documents/nr-reporting-summary-flat.pdf

Life sciences study design

All studies must disclose on these points even when the disclosure is negative.

Sample size	<p>Sample sizes were based on comparable n-values from the literature published previously, as shown below.</p> <p>Wong, L.C., Wang, L., D'Amour, J.A., Yumita, T., Chen, G., Yamaguchi, T., Chang, B.C., Bernstein, H., You, X., Feng, J.E., et al. (2016). Effective Modulation of Male Aggression through Lateral Septum to Medial Hypothalamus Projection. <i>Current biology</i> : CB 26, 593-604. 10.1016/j.cub.2015.12.065.</p> <p>Yin, L., Hashikawa, K., Hashikawa, Y., Osakada, T., Lischinsky, J.E., Diaz, V., and Lin, D. (2022). VMHvlCckar cells dynamically control female sexual behaviors over the reproductive cycle. <i>Neuron</i> 110, 3000-3017.e3008. https://doi.org/10.1016/j.neuron.2022.06.026.</p> <p>Yamaguchi, T., Wei, D., Song, S.C., Lim, B., Tritsch, N.X., and Lin, D. (2020). Posterior amygdala regulates sexual and aggressive behaviors in male mice. <i>Nat Neurosci</i> 23, 1111-1124. 10.1038/s41593-020-0675-x.</p> <p>Falkner, A.L., Wei, D., Song, A., Watsek, L.W., Chen, I., Chen, P., Feng, J.E., and Lin, D. (2020). Hierarchical Representations of Aggression in a Hypothalamic-Midbrain Circuit. <i>Neuron</i> 106, 637-648 e636. 10.1016/j.neuron.2020.02.014.</p> <p>Fang, Y.Y., Yamaguchi, T., Song, S.C., Tritsch, N.X., and Lin, D. (2018). A Hypothalamic Midbrain Pathway Essential for Driving Maternal Behaviors. <i>Neuron</i> 98, 192-207 e110. 10.1016/j.neuron.2018.02.019.</p>
Data exclusions	<p>Mice failing to display aggression within three days (one RI test/day) were excluded in most of experiments, except experiments in Figure 1l-w, Figure 2a-e, Extended Data Figure 4, Extended Data Figure 5, Extended Data Figure 6b,e, f-i, Extended Data Figure 7, Extended Data Figure 8i-k.</p> <p>In Figure 1, 6 DAT-cre male mice with hM4Di have been excluded from the experiments due to the different experiment design.</p> <p>In Figure 2f-n, 2 mouse was excluded due to the misplacement of optic fibers.</p> <p>During slice recording, cells were excluded if the access resistance was higher than 20 MΩ at the end of recording. For current-clamp recording, cells were excluded if the holding current was lower than -50 pA at -70 mV. For voltage-clamp recording, cells were excluded if the holding current was lower than -200 pA at -70 mV.</p> <p>In Figure 3h-m, 8 cells from 3 mice in ACSF group and 9 cells from 3 mice in Sul group were excluded because we did not record sIPSC for long</p>

enough time after terminal stimulation.

In Figure 3q-t, 20 cells from 3 mice in novice and 25 cells from 5 mice in expert condition were excluded due to lack of SUM application.

In Figure 3u-w, 17 cells from 3 mice in novice and 28 cells from 4 mice in expert condition were excluded due to lack of SUM application.

Replication

All functional and fiber photometry recording experiments started with a small batch of test (and control) animals (2–4 animals per group) and then gradually added more animals for each group as transgenic mice became available. We made sure that control and test mice were added around the same time. The final analysis for each experiment combined all animals from different cohorts. Chemogenetic activation of VMH *Esr1* cells in ExFig 2, RNA scope data in Fig 3bb-dd, DA3h recording in social interaction group in ExFig 7a-g, c-fos induction in ExFig 8k, DA terminal activation at NAc in ExFig 8k-s, was collected at once for all the animals.

Randomization

Mice were randomly assigned to experimental groups (such as mCherry, hM4Di, or hM3Dq group in Fig1a-k, sgRosa26 vs sgTH in Fig1l-w, 6-OHDA vs vehicle injection in NAc or dLS, in Fig 2a-e, EYFP vs ChR2 in Fig 2o-y). For chemogenetic experiments, half of the animals were randomly assigned to receive C21 first, the other half received saline first.

Blinding

The c-Fos quantification and histology analysis were completed by experienced researchers who are blind to the treatment. Other experiments were performed by experimenters who are not blind to the group allocation during data acquisition or analysis. We make sure that control and experiments group were test in the same condition, and data were analyzed with the same criteria. Aggressive behaviors were analyzed primarily using automated behavior recognition software, Simba, followed by manual checking by researchers either blind or not blind to the treatment conditions.

Reporting for specific materials, systems and methods

We require information from authors about some types of materials, experimental systems and methods used in many studies. Here, indicate whether each material, system or method listed is relevant to your study. If you are not sure if a list item applies to your research, read the appropriate section before selecting a response.

Materials & experimental systems

- | | | |
|-------------------------------------|-------------------------------------|-------------------------------|
| n/a | <input type="checkbox"/> | Included in the study |
| <input type="checkbox"/> | <input checked="" type="checkbox"/> | Antibodies |
| <input checked="" type="checkbox"/> | <input type="checkbox"/> | Eukaryotic cell lines |
| <input checked="" type="checkbox"/> | <input type="checkbox"/> | Palaeontology and archaeology |
| <input type="checkbox"/> | <input checked="" type="checkbox"/> | Animals and other organisms |
| <input checked="" type="checkbox"/> | <input type="checkbox"/> | Clinical data |
| <input checked="" type="checkbox"/> | <input type="checkbox"/> | Dual use research of concern |
| <input checked="" type="checkbox"/> | <input type="checkbox"/> | Plants |

Methods

- | | | |
|-------------------------------------|--------------------------|------------------------|
| n/a | <input type="checkbox"/> | Included in the study |
| <input checked="" type="checkbox"/> | <input type="checkbox"/> | ChIP-seq |
| <input checked="" type="checkbox"/> | <input type="checkbox"/> | Flow cytometry |
| <input checked="" type="checkbox"/> | <input type="checkbox"/> | MRI-based neuroimaging |

Antibodies

Antibodies used

Primary antibodies used were: chicken anti-GFP antibody (1:1000, Abcam, ab13970), rabbit anti-dsRed antibody (1:1000, Takara, 632496), sheep anti-TH primary antibody (1:750, Pel Freeze, P60101-0), rabbit anti-TH primary antibody (1:500, EMD Millipore, AB152), guinea pig anti-c-fos antibody (1:1000, SYSY, 226308). Secondary antibodies used were: Alexa 488-conjugated donkey anti-chicken secondary antibody (1:1000, Jackson ImmunoResearch, 703-545-155), Cy3-conjugated donkey anti-rabbit secondary antibody (1:1000, Jackson ImmunoResearch, 711-165-152), Alexa 488-conjugated donkey anti-sheep secondary antibody (1:1000, Jackson ImmunoResearch, 713-545-147), Cy3-conjugated donkey anti-rabbit secondary antibody (1:1,000), Cy3-conjugated donkey anti-guinea pig secondary antibody (1:1000, Jackson ImmunoResearch, 706-165-148) .

Validation

All the antibodies used in this paper have been used in our previous studies and cited multiple times as listed on the manufacture's website or CiteAb([https:// www.citeab.com/](https://www.citeab.com/)).

Specifically, for the primary antibodies used in this paper,

chicken anti-GFP antibody (1:1000, Abcam, ab13970): Dai, B., et al., Cell Reprints 2022.

rabbit anti-dsRed antibody (1:1000, Takara, 632496): Grippo, R., et al. Current Biology 2017; Nicolai, L., et al. PNAS 2010.

sheep anti-TH primary antibody (1:750, Pel Freeze, P60101-0): Dai, B., et al., Cell Reprints 2022.

rabbit anti-TH primary antibody (1:500, EMD Millipore, AB152): McNamara, C., et al. Nature neuroscience 2014.

guinea pig anti-c-fos antibody (1:1000, SYSY, 226308): Osakada, T., et al. Nature 2024.

Animals and other research organisms

Policy information about [studies involving animals](#); [ARRIVE guidelines](#) recommended for reporting animal research, and [Sex and Gender in Research](#)

Laboratory animals

All procedures were approved by the NYULMC Institutional Animal Care and Use Committee (IACUC) in compliance with the National Institutes of Health (NIH) Guidelines for the Care and Use of Laboratory Animals. Mice were housed under a 12-hour light-dark cycle (dark cycle; 10 a.m. to 10 p.m. or 6:30 p.m. to 6:30 a.m.), with food and water available ad libitum. Room temperature was maintained between 20–22°C and humidity between 30–70%, with a daily average of approximately 45%. Test animals were adult DAT-cre (Jackson, 006660), Drd2-cre (MMRRC_032108-UCD), *Esr1-2A-cre* (Jackson, 017911), and WT C57BL6/N (Charles River, 027) mice. They were between 8 and 20 weeks old at the time of behavior testing or recording. Intruder animals in the inter-male RI tests were adult Balb/C (>8 weeks) male mice. During each RI test, the intruder was randomly picked from a group of 20-30 mice, housed

4-5 mice/cage. For the male-female RI test, adult C57BL/6N or Balb/C (>8 weeks) female mice were used. For the female aggression test, juvenile C57BL/6N (approximately 21-28 days old) male mice were used. All intruder mice were originally purchased from Charles River and then bred in-house. They were group-housed until adulthood. Females were considered receptive if an experienced male could mount and intromit the female within three attempts. After surgery, all male test mice were single-housed, while female test mice were paired with adult male mice until the females became visibly pregnant. Animals were randomly assigned to control and test groups. All experiments were performed during the dark cycle of the animals.

Wild animals

The study did not involve wild animals.

Reporting on sex

Stimulus animals in the RI tests were adult C57BL/6N (>8 weeks) and Balb/C (>8 weeks) male and female mice originally purchased from Charles River and then bred in-house. Both male and female DAT-cre C57BL/6N mice were used as test animals for the initial validation of the VTA dopamine cells' role in aggression, but only male *Drd2-cre*, *Esr1-2A-cre*, and WT C57BL/6N mice were used in later experiments.

Field-collected samples

The study did not involve field collected samples

Ethics oversight

All procedures were approved by the NYULMC Institutional Animal Care and Use Committee (IACUC) in compliance with the National Institutes of Health (NIH) Guidelines for the Care and Use of Laboratory Animals.

Note that full information on the approval of the study protocol must also be provided in the manuscript.

Plants

Seed stocks

N/A

Novel plant genotypes

N/A

Authentication

N/A